

# Realization of microwave amplification, attenuation, and frequency conversion using a single three-level superconducting quantum circuit

Yan-Jun Zhao,<sup>1,2,3</sup> Jiang-Hao Ding,<sup>1</sup> Z. H. Peng,<sup>4</sup> and Yu-xi Liu<sup>1,5,\*</sup>

<sup>1</sup>*Institute of Microelectronics, Tsinghua University, Beijing 100084, China*

<sup>2</sup>*Beijing National Laboratory for Condensed Matter Physics*

<sup>3</sup>*Institute of Physics, Chinese Academy of Sciences, Beijing 100190, China*

<sup>4</sup>*CEMS, RIKEN, Saitama 351-0198, Japan*

<sup>5</sup>*Tsinghua National Laboratory for Information Science and Technology (TNList), Beijing 100084, China*

(Dated: March 6, 2022)

Using different configurations of applied strong driving and weak probe fields, we find that only a single three-level superconducting quantum circuit (SQC) is enough to realize amplification, attenuation and frequency conversion of microwave fields. Such a three-level SQC has to possess  $\Delta$ -type cyclic transitions. Different from the parametric amplification (attenuation) and frequency conversion in nonlinear optical media, the real energy levels of the three-level SQC are involved in the energy exchange when these processes are completed. We quantitatively discuss the effects of amplification (attenuation) and the frequency conversion for different types of driving fields. The optimal points are obtained for achieving the maximum amplification (attenuation) and conversion efficiency. Our study provides a new method to amplify (attenuate) microwave, realize frequency conversion, and also lay a foundation for generating single or entangled microwave photon states using a single three-level SQC.

PACS numbers: 42.65.Es, 42.65.Ky, 75.30.Cr

## I. INTRODUCTION

Three-wave mixing is very fundamental in nonlinear quantum optics [1]. It can be used to generate single photon or entangled photon pairs. Three-wave mixing can also be used to convert the frequency of the weak electromagnetic field or amplify the weak electromagnetic signal by virtue of another strong driving field. In atomic systems with inversion symmetry, the three-wave mixing can only occur in a parametric way because of the selection rule in the electric-dipole interaction between the atoms and electric fields. Thus, the nonlinear interaction strength of the three-wave mixing is usually weak in the natural atomic systems. In contrast to the parametric weak nonlinearity realized by the virtual single- or two-photon processes, the nonlinear interaction strength can be increased significantly when the real energy exchange is involved. For example, in molecular systems [2–4], the inversion symmetry can be broken, and the transitions between any two energy levels are possible. In such cases, the three-wave mixing processing can be realized using real energy transitions between energy levels. In artificial atoms, e.g., semiconducting quantum dots or superconducting quantum circuits (SQCs), the inversion symmetry of their potential energy can be artificially controlled by externally applied field, that is, the selection rule of the artificial atoms can be engineered. Thus, they provide us a new platform to manipulate and engineer linear and nonlinear quantum processes. For example, the single photon strong coupling can be achieved between

microwave and mechanical modes using a superconducting flux qubit [5]. It is also possible to realize three-wave mixing using real energy transitions between energy levels of a single SQC [6].

The SQCs [7–13] are extensively explored for the realization of qubits which are basic building blocks of quantum information processing. These superconducting artificial atoms can also be used not only to demonstrate phenomena occurred in atomic physics and quantum optics, but also to show some novel results, which cannot be found in natural atomic systems. For example, the dressed states [14, 15] have been experimentally demonstrated using superconducting charge qubit circuits [16, 17]. The Autler-Townes splitting [18–24] and coherent population trapping [25] have also been observed in three-level SQCs. Experimentalists are trying to find a way to realize the electromagnetically induced transparency in varieties of three-level superconducting quantum devices [26–30]. Moreover, the coexistence of single- and two-photon processes [31] in three-level superconducting flux qubit circuits [31, 32] has been experimentally demonstrated [33] by designed circuit QED systems. However, such phenomenon cannot be demonstrated using three-level natural atoms because of the electric-dipole transition rule.

The microwave amplification has been experimentally demonstrated by a single three-level artificial atom in open one-dimensional space [34], a dressed [35] or a doubly-dressed superconducting flux [36] qubit circuit. The coherent frequency conversion has been demonstrated using two internal degrees of freedom of a single dc-SQUID phase qubit circuit [37]. The parametric down conversion and squeezing of two-mode quantized microwave fields using circuit QED are theoretic-

---

\*Electronic address: yuxiliu@mail.tsinghua.edu.cn

cally studied [38]. Moreover, the parametric three-wave mixing devices have also been experimentally demonstrated [39, 40]. It was shown that the amplifiers with single artificial atoms [34] are different from the Josephson junction based parametric three-wave mixing devices [39, 40] or amplifiers [41–44]. A main difference is that the real energy exchange between discrete energy levels is involved when the single artificial atom amplifiers are implemented. We recently showed that a three-level flux qubit circuits [6] with  $\Delta$ -type cyclic transitions can be used to generate three-wave mixing.

Motivated by the work [6, 34], we now give a detailed study on the microwave amplification and frequency conversion by a single three-level SQC with  $\Delta$ -type transitions, which can be realized by superconducting flux [31, 32], phase [45–47], fluxonium [48, 49] or Xmon qubit circuits [50]. For concreteness, we here focus on flux qubit circuits. In our study, we mainly study the conversion efficiency and the amplification and attenuation of the weak signal field. Our paper is organized as follows. In Sec. II, we give an overview of the theoretical model. In Sec. III, we study the microwave attenuation and frequency conversion for driving type (1). In Sec. IV, we study the same contents for driving type (2). In Sec. V, we study microwave amplification, attenuation, and frequency conversion for driving type (3). Finally, we summarize our results and discuss both measurements and experimental feasibilities.

## II. THEORETICAL MODEL OVERVIEW

We study microwave amplifications, attenuation and frequency conversions in a three-level superconducting artificial atom with  $\Delta$ -type transitions [31], as schematically shown in Fig. 1(a). The three energy levels are denoted by  $|1\rangle$ ,  $|2\rangle$ , and  $|3\rangle$ . Here, we specify our study to superconducting flux qubit circuits, typically consisting of three Josephson junctions [31, 32]. We assume that the bias magnetic flux is not at the optimal point so that the three energy levels chosen from such circuit can possess  $\Delta$ -type transition when the external fields are applied. We also assume that the three-level system is placed inside an open one-dimensional transmission line resonator as in Ref. [34]. Hereafter, for simplicity, we use three-level systems to denote such three-level superconducting flux qubit circuits.

To realize the microwave amplification, attenuation, or frequency conversion, a strong driving field has to be applied to the three-level system with  $\Delta$ -type transitions, as shown in Figs. 1(b), (c) and (d), the strong driving field can be applied to couple: (1) the energy levels  $|1\rangle$  and  $|2\rangle$ ; or (2) the energy levels  $|2\rangle$  and  $|3\rangle$ ; or (3) the energy levels  $|1\rangle$  and  $|3\rangle$ . Corresponding to each configuration of the driving field, the signal field can be applied in two ways. For example, as shown in two panels of Fig. 1(b), the signal field can be applied to either the energy levels  $|1\rangle$  and  $|3\rangle$  (shown in up panel of Fig. 1(b)),

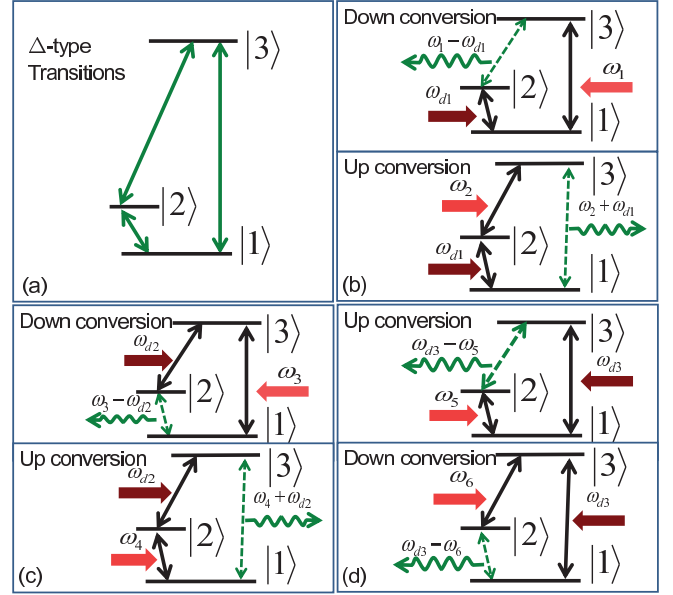


FIG. 1: Schematic diagram for three-level superconducting quantum circuits with the  $\Delta$ -type transitions in (a). The driving field has three different ways to be applied for attenuation, amplification, or frequency conversion processes as shown in (b), (c) and (d). Each of three figures includes two panels, corresponding to up and down frequency conversions, respectively. In all the three figures, the light red arrows mean the signal field. However, the dark red arrows mean the strong driving field. The green arrows denote the converted signal.

or the energy levels  $|2\rangle$  and  $|3\rangle$  (shown in down panel of Fig. 1(b)) when the driving field is applied to the energy levels  $|1\rangle$  and  $|2\rangle$ .

In strong driving types (1) and (2) as shown in Figs. 1(b) and (c), the frequency down or up conversion can be realized by properly applying the signal field. But in the driving type (3) as shown in Fig. 1(d), the up and down conversions are a little bit different from the types (1) and (2). In the types (1) and (2), the down (up) frequency conversion is the difference between (sum of) frequencies of the signal and driving fields. However, in the type (3), both the down and up frequency conversions are the difference between the frequencies of signal and driving fields, when the frequency difference is larger than the signal frequency, we call this process as the up conversion, otherwise the down conversion.

In all three driving ways with applied signal fields, the total Hamiltonian can be generally given by

$$H^{(l)} = \hbar\omega_{21}\sigma_{22} + \hbar\omega_{31}\sigma_{33} + H_R^{(l)} + H_{pk}^{(l)} + H_T^{(l)}, \quad (1)$$

from Ref. [6] when one of the weak fields is replaced by a strong field. We note that we sometimes also call signal fields as probing fields. Hereafter,  $\sigma_{mn} = |m\rangle\langle n|$  with  $n, m = 1, 2$ , or  $3$ . The superscript  $l = 1, 2$ , or  $3$  is used to represent different driving types. The Hamiltonian  $H^{(l)}$  can be exemplified by the circuit schematic in Fig. 2 where the signals applied through the transmission line

TABLE I: Summary of the interaction Hamiltonian  $H_R^{(l)}(t)$  between the three-level superconducting artificial atoms and the strong driving field, which can be applied to the three-level systems in three different ways. Corresponding to each strong driving field, the probe fields can be applied to the three-level system in two different ways with interaction Hamiltonians  $H_{pk}^{(l)}(t)$  where  $k = 2l - 1$  or  $2l$  respectively. Here,  $\hbar\Omega_{mn,l} = -MI_{mn}\tilde{I}_{dl}/2$ . The incident driving current is assumed as  $I_{dl}(x, t) = \text{Re}[\tilde{I}_{dl}e^{-i\omega_{dl}(t-x/v)}]$  where  $l = 1, 2$ , or  $3$ , and  $x$  is the position coordinate. The incident signal currents are assumed as  $I_{pk}(x, t) = \text{Re}[\tilde{I}_{pk}e^{-i\omega_k(t-x/v)}]$  with phase velocity  $v$ . The parameter  $\hat{I}$  is the loop current of the flux qubit circuit and  $I_{mn}$  is its matrix element in the energy basis.

Driving type	Interaction Hamiltonian with the driving field	Interaction Hamiltonian with the probe field
Type (1)	$H_R^{(1)}(t) = \hbar[\Omega_{21,1}\sigma_{21}\exp(-i\omega_{d1}t) + \text{H.c.}]$	$H_{p1}^{(1)}(t) = -M\hat{I}I_{p1}(0, t)$ $H_{p2}^{(1)}(t) = -M\hat{I}I_{p2}(0, t)$
Type (2)	$H_R^{(2)}(t) = \hbar[\Omega_{32,2}\sigma_{32}\exp(-i\omega_{d2}t) + \text{H.c.}]$	$H_{p3}^{(2)}(t) = -M\hat{I}I_{p3}(0, t)$ $H_{p4}^{(2)}(t) = -M\hat{I}I_{p4}(0, t)$
Type (3)	$H_R^{(3)}(t) = \hbar[\Omega_{31,3}\sigma_{31}\exp(-i\omega_{d3}t) + \text{H.c.}]$	$H_{p5}^{(3)}(t) = -M\hat{I}I_{p5}(0, t)$ $H_{p6}^{(3)}(t) = -M\hat{I}I_{p6}(0, t)$

will be scattered by the flux qubit as in Ref. [58]. In the type of the  $l$ th driving, the symbol  $H_R^{(l)} \equiv H_R^{(l)}(t)$  (or  $H_{pk}^{(l)} \equiv H_{pk}^{(l)}(t)$ ) denotes the interaction Hamiltonian between the strong driving field (or the weak signal field) and the three-level system. The Hamiltonian

$$H_T^{(l)} \equiv H_T^{(l)}(t) = -M\hat{I}(I_L(0, t) + I_R(0, t)) \quad (2)$$

describes the interaction between the three-level system and environment in open one-dimensional transmission line. In Eq. (2), we have used the two following symbols

$$I_L(x, t) = -\int_{-\infty}^{\infty} d\omega g(\omega) A_L(\omega) e^{-i\omega(t-x/v)}, \quad (3)$$

$$I_R(x, t) = \int_{-\infty}^{\infty} d\omega g(\omega) A_R(\omega) e^{-i\omega(t+x/v)}, \quad (4)$$

with  $g(\omega) = i \text{sgn}(\omega) \sqrt{\hbar|\omega|/4\pi Z_T}$  for the noise currents coming from the left and right. The parameter  $Z_T$  represents the characteristic impedance of the transmission line. The commutation relations of  $A_\alpha(\omega)$  are  $[A_\alpha(\omega_1), A_\alpha(\omega_2)] = \delta(\omega_1 + \omega_2) \text{sgn}(\omega_1)$  for  $\alpha = L$  or  $R$ . Without the driving fields, the relaxation rates of the

three-level system are proportional to the parameters

$$\lambda_{mn} = I_{mn}^2 \omega_{mn}, m > n. \quad (5)$$

All the types of interaction Hamiltonians  $H_R^{(l)}(t)$  and  $H_{pk}^{(l)}(t)$  have been summarized in Table I.

Our research is based on the following hypotheses. (1) The intrinsic loss of the three-level system is negligible. Hence, the 1D open space determines the total decay rates. (2) The frequency shifts induced by the driving field are much larger than the decay rates but still negligibly small compared to the original eigen frequencies of the three-level system. (3) The interaction Hamiltonian between the flux qubit circuit and the probe field  $H_{pk}^{(l)}(t)$  is a small quantity compared with that between the flux qubit circuit and the driving field  $H_R^{(l)}(t)$ . Thus, the response to the probe signal can be solved using linear response theory [1]. (4) The environment temperature is too enough to induce effective dephasing or thermal excitation.

Below we will first use driving type (1) as an example to show detailed derivations. The treatments in driving type (2) and (3) are similar to that in driving type (1).

### III. MICROWAVE ATTENUATION AND FREQUENCY CONVERSIONS FOR DRIVING TYPE (1)

#### A. Hamiltonian reduction

In the driving type (1), the Hamiltonian  $H_R^{(1)}(t)$  can be given as

$$H_R^{(1)}(t) = \hbar\Omega_{21,1}\sigma_{21}\exp(-i\omega_{d1}t) + \text{H.c.} \quad (6)$$

with  $\Omega_{21,1} = -MI_{21}\tilde{I}_{d1}/2$ . Here  $M$  is the mutual inductance, and  $I_{mn}$  is the matrix element of the loop current  $\hat{I}$  of the three-level superconducting flux qubit circuit. The incident driving current is assumed as  $I_{d1}(x, t) = \text{Re}[\tilde{I}_{d1}e^{-i\omega_{d1}(t-x/v)}]$  with phase velocity  $v$ . We assume that the three-level system is placed at the position of  $x = 0$  and also  $\Omega_{21,1}$  is a real number without loss of generality.

Corresponding to the Hamiltonian in Eq. (6), the

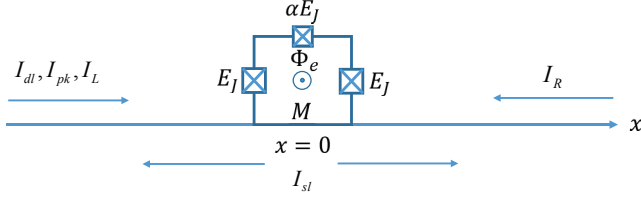


FIG. 2: Schematic diagram for a typical experimental circuit. The three-junction flux qubit is coupled to an one-dimensional open transmission line by a edge-sharing mutual inductance  $M$ . The qubit is also biased by a DC magnetic flux  $\Phi_e$ . The location on the transmission line is denoted by  $x$  with the qubit placed at  $x = 0$ . The incident driving and probing currents are respectively denoted by  $I_{dl} \equiv I_{dl}(x, t)$  and  $I_{pk} \equiv I_{pk}(x, t)$ . The scattered current is  $I_{sl} \equiv I_{sl}(x, t)$ . Here, the values of  $k = 2l - 1$  or  $2l$ . The quantum noise currents come from both directions are respectively  $I_L = I_L(x, t)$  and  $I_R = I_R(x, t)$ . The Josephson energies (capacitances) of the two identical junctions and the smaller one are  $E_J$  ( $C$ ) and  $\alpha E_J$  ( $\alpha C$ ) with  $0.5 < \alpha < 1$ , respectively. Here,  $E_C = e^2/2C$  is called the charging energy with the electron charge  $e$ . In addition, the characteristic impedance of the transmission line is assumed as  $Z_T$ .

Hamiltonian  $H_{pk}^{(1)}(t)$  with  $k = 1$  or  $2$  are respectively

$$H_{p1}^{(1)}(t) = -M\hat{I}_{p1}(0, t), \quad (7)$$

$$H_{p2}^{(1)}(t) = -M\hat{I}_{p2}(0, t), \quad (8)$$

without the rotating wave approximation (RWA). The Hamiltonian in Eq. (1) with  $H_R^{(1)}(t)$  in Eq. (6) and  $H_{p1}^{(1)}(t)$  in Eq. (7) describes the frequency down conversion as shown in the up panel of Fig. 1(b). However, the Hamiltonian  $H_{p2}^{(1)}(t)$  can be written as for that the signal field is applied to the energy levels  $|2\rangle$  and  $|3\rangle$ . That is, the Hamiltonian in Eq. (1) with  $H_R^{(1)}(t)$  in Eq. (6) and  $H_{p2}^{(1)}(t)$  in Eq. (8) describes the frequency up conversion as shown in the down panel of Fig. 1(b). The incident signal currents are assumed as  $I_{pk}(x, t) = \text{Re}[\tilde{I}_{pk}e^{-i\omega_k(t-x/v)}]$  with  $k = 1$  or  $k = 2$ .

To remove the time dependence of  $H^{(1)}$ , we now use a unitary transformation  $U_d^{(1)} = \exp(-i\omega_{d1}t\sigma_{22})$ . Then at a frame rotating, we get an effective Hamiltonian

$$H_{\text{eff}}^{(1)} = \hbar\Delta_{21,1}\sigma_{22} + \hbar\omega_{31}\sigma_{33} + \hbar\Omega_{21,1}(\sigma_{21} + \sigma_{12}) - M\hat{I}^{(1)}(t)I_{pk}(0, t) - M\hat{I}^{(1)}(t)(I_L(0, t) + I_R(0, t)), \quad (9)$$

with driving detuning  $\Delta_{21,1} = \omega_{21} - \omega_{d1}$  and the transformed loop current  $\hat{I}^{(1)}(t) = U_d^{(1)\dagger}\hat{I}U_d^{(1)}$ . Since we have assumed a strong driving strength  $\Omega_{mn,l}$ , it is reasonable to work in the eigen basis of the first three terms of Eq. (9). For this consideration, we apply to  $H_{\text{eff}}^{(1)}$  a unitary transformation  $U_r^{(1)} = \exp[-i\theta_1(-i\sigma_{21} + i\sigma_{12})/2]$  with  $\tan\theta_1 = 2\Omega_{21,1}/\Delta_{21,1}$ , yielding

$$\bar{H}_{\text{eff}}^{(1)} = U_r^{(1)\dagger}H_{\text{eff}}^{(1)}U_r^{(1)} = H_S^{(1)} + \bar{H}_{pk}^{(1)} + H_T^{(1)}. \quad (10)$$

The symbols  $H_S^{(1)}$ ,  $\bar{H}_{pk}^{(1)}$ ,  $H_T^{(1)}$  respectively take the following forms, i.e.,

$$H_S^{(1)} = \hbar\omega_1^{(1)}\sigma_{11} + \hbar\omega_2^{(1)}\sigma_{22} + \hbar\omega_3^{(1)}\sigma_{33}, \quad (11)$$

$$\bar{H}_{pk}^{(1)} = -M\bar{I}^{(1)}(t)I_{pk}(0, t), \quad (12)$$

$$H_T^{(1)} = -M\bar{I}^{(1)}(t)(I_L(0, t) + I_R(0, t)). \quad (13)$$

Note that  $\bar{I}^{(1)}(t) = U_r^{(1)\dagger}\hat{I}^{(1)}(t)U_r^{(1)}$  is another transformed loop current. Its matrix elements  $\bar{I}_{mn}^{(1)}(t)$  have been listed in Appendix. A. The Hamiltonian  $H_S^{(1)}$  is defined as the system Hamiltonian originating from the first three terms of  $H_{\text{eff}}^{(1)}$  in Eq. (9). In Eq. (11), the eigen frequencies of the system Hamiltonian are respectively represented as

$$\omega_1^{(1)} = \frac{1}{2}\left(\Delta_{21,1} - \sqrt{4\Omega_{21,1}^2 + \Delta_{21,1}^2}\right), \quad (14)$$

$$\omega_2^{(1)} = \frac{1}{2}\left(\Delta_{21,1} + \sqrt{4\Omega_{21,1}^2 + \Delta_{21,1}^2}\right), \quad (15)$$

$$\omega_3^{(1)} = \omega_{31}. \quad (16)$$

The Hamiltonian  $\bar{H}_{pk}^{(1)}$  is a small quantity compared to  $H_S^{(1)}$  and hence will be treated as a perturbation in the following discussions. And  $H_T^{(1)}$  represents the interaction between the system and 1D open space. With fast oscillating terms neglected,  $\bar{H}_{pk}^{(1)}$  can be further reduced to

$$\bar{H}_{p1} = \hbar\varepsilon_{31,1}e^{-i\omega_1 t}\sigma_{31} + \hbar\varepsilon_{32,1}e^{-i\omega_1 t}\sigma_{32} + \text{h.c.}, \quad (17)$$

$$\bar{H}_{p2} = \hbar\varepsilon_{31,2}e^{-i\omega_2 t}\sigma_{31} + \hbar\varepsilon_{32,2}e^{-i\omega_2 t}\sigma_{32} + \text{h.c.} \quad (18)$$

Here,  $\omega_{2+} = \omega_2 + \omega_{d1}$  is the produced sum frequency, and

$$\hbar\varepsilon_{31,1} = -\frac{1}{2}M\cos\frac{\theta_1}{2}\tilde{I}_{p1}I_{31}, \quad (19)$$

$$\hbar\varepsilon_{32,1} = -\frac{1}{2}M\sin\frac{\theta_1}{2}\tilde{I}_{p1}I_{31}, \quad (20)$$

$$\hbar\varepsilon_{31,2} = \frac{1}{2}M\sin\frac{\theta_1}{2}\tilde{I}_{p2}I_{32}, \quad (21)$$

$$\hbar\varepsilon_{32,2} = -\frac{1}{2}M\cos\frac{\theta_1}{2}\tilde{I}_{p2}I_{32}, \quad (22)$$

are the coupling energy parameters.

## B. Dynamics of the system and its solutions

Using the detailed parameters of  $\bar{I}^{(1)}(t)$  in Appendix. A, we can derive that the reduced density matrix  $\rho$  of the system is governed by the following master equation [55]

$$\frac{\partial\rho}{\partial t} = \frac{1}{i\hbar}[H_S^{(1)} + \bar{H}_{pk}^{(1)}, \rho] + \mathcal{L}[\rho]. \quad (23)$$

We must mention we work in the picture defined by unitary transformations  $U_d^{(1)}$  and  $U_r^{(1)}$ . The dissipation of the system is described via the Lindblad term

$$\mathcal{L}[\rho] = \sum_m \left( \sum_{k \neq m} \gamma_{km}^{(1)} \rho_{kk} - \sum_{k \neq m} \gamma_{mk}^{(1)} \rho_{mm} \right) \sigma_{mm} - \sum_{m \neq n} \frac{1}{2} \Gamma_{mn}^{(1)} \rho_{mn} \sigma_{mn}. \quad (24)$$

Here,  $\rho_{mn} \equiv \rho_{mn}(t)$  are matrix elements of the reduced density operator  $\rho(t)$ . The relaxation and dephasing rates can be calculated as  $\gamma_{mn}^{(1)} = \frac{M^2}{\hbar Z_T} K_{mn}^{(1)}$  and  $\Gamma_{mn}^{(1)} = \frac{M^2}{\hbar Z_T} \left( \sum_{k \neq m} K_{mk}^{(1)} + \sum_{k \neq n} K_{nk}^{(1)} + K_{\phi mn}^{(1)} \right)$  from hypotheses (1), (2), and (4) in Sec. II. The explicit expressions of  $K_{mn}^{(1)}$  and  $K_{\phi mn}^{(1)}$  are given in Appendix A.

It is not easy to obtain the exact solutions of the nonlinear equations in Eq. (23) because the steady state response contains infinite components of different frequencies in nonlinear systems. Thus, as extensively used method in nonlinear optics [1], we now seek the solutions of Eq. (23) in the form of a power series expansion in the magnitude of  $\bar{H}_{pk}^{(1)}$ , that is, a solution of the form

$$\rho(t) = \rho^{(0)} + \rho^{(1)}(t) + \dots + \rho^{(r)}(t) + \dots, \quad (25)$$

for the reduced density matrix  $\rho$  of the three-level system. Here,  $\rho^{(0)}$  is the steady state solution when no signal field is applied to the system. However the  $r$ th-order reduced density matrix  $\rho^{(r)}(t)$  is proportional to  $r$ th order of  $\bar{H}_{pk}^{(1)}$ .

In the first order approximation, we have

$$\frac{\partial \rho^{(0)}}{\partial t} = \frac{1}{i\hbar} [H_S^{(1)}, \rho^{(0)}] + \mathcal{L}[\rho^{(0)}], \quad (26)$$

$$\frac{\partial \rho^{(1)}}{\partial t} = \frac{1}{i\hbar} [H_S^{(1)}, \rho^{(1)}] + \frac{1}{i\hbar} [\bar{H}_{pk}^{(1)}, \rho^{(0)}] + \mathcal{L}[\rho^{(1)}]. \quad (27)$$

The solutions of Eq. (26) is

$$\rho_{11}^{(0)} = \frac{1}{1 + y_1^2}, \quad (28)$$

$$\rho_{22}^{(0)} = \frac{y_1^2}{1 + y_1^2}, \quad (29)$$

with  $y_1 = \tan^2(\theta_1/2)$ . And the other terms of  $\rho^{(0)}$  are all zeros. Having obtained  $\rho^{(0)}$ , we can further solve Eq. (27). When  $\bar{H}_{pk}^{(1)}$  takes  $\bar{H}_{p1}^{(1)}$ , we have the nonzero matrix elements of  $\rho^{(1)}$  as follows,

$$\rho_{31}^{(1)} = \rho_{13}^{(1)*} = \frac{-i\varepsilon_{31,1} e^{-i\omega_1 t}}{i(\omega_{31}^{(1)} - \omega_1) + \frac{1}{2}\Gamma_{31}^{(1)}} \rho_{11}^{(0)}, \quad (30)$$

$$\rho_{32}^{(1)} = \rho_{23}^{(1)*} = \frac{-i\varepsilon_{32,1} e^{-i\omega_1 t}}{i(\omega_{32}^{(1)} - \omega_1) + \frac{1}{2}\Gamma_{32}^{(1)}} \rho_{22}^{(0)}. \quad (31)$$

When  $\bar{H}_{pk}^{(1)}$  takes  $\bar{H}_{p2}^{(1)}$ , we have the nonzero matrix elements of  $\rho^{(1)}$  as follows,

$$\rho_{31}^{(1)} = \rho_{13}^{(1)*} = \frac{-i\varepsilon_{31,2} e^{-i\omega_2 t}}{i(\omega_{31}^{(1)} - \omega_{2+}) + \frac{1}{2}\Gamma_{31}^{(1)}} \rho_{11}^{(0)}, \quad (32)$$

$$\rho_{32}^{(1)} = \rho_{23}^{(1)*} = \frac{-i\varepsilon_{32,2} e^{-i\omega_2 t}}{i(\omega_{32}^{(1)} - \omega_{2+}) + \frac{1}{2}\Gamma_{32}^{(1)}} \rho_{22}^{(0)}. \quad (33)$$

### C. Scattered current

The noise current ( $I_L$  and  $I_R$ ) will induce the scattered current of the classical fields through interaction with the three-level system. Using the input-output theory extensively discussed in Refs. [52–56], the scattered current at  $x = 0$  can be represented by

$$I_{s1}(0, t) = -\frac{iM}{2Z_T} \sum_{mnk} \delta_{mnk}^{(1)} \bar{I}_{mnk}^{(1)} e^{i\nu_{mnk}^{(1)} t} \rho_{nm}, \quad (34)$$

with  $\delta_{mnk}^{(1)} = \omega_{mn}^{(1)} + \nu_{mnk}^{(1)}$ , and  $\omega_{mn}^{(1)} = \omega_m^{(1)} - \omega_n^{(1)}$ . Here, we have assumed that the matrix element of  $\bar{I}^{(1)}(t)$  is of the form  $\bar{I}_{mn}^{(1)}(t) = \sum_k \bar{I}_{mnk}^{(1)} e^{i\nu_{mnk}^{(1)} t}$ . The scattered current can also be expanded in the order of  $\bar{H}_{pk}^{(1)}$ , i.e.,  $I_{s1} = \sum_{r=0}^{\infty} I_{s1}^{(r)}$ . Here, we only care about the linear response in the expansion of  $I_{s1}$ , that is,

$$I_{s1}^{(1)}(0, t) = -\frac{iM}{2Z_T} \sum_{mnk} \delta_{mnk}^{(1)} \bar{I}_{mnk}^{(1)} e^{i\nu_{mnk}^{(1)} t} \rho_{nm}^{(1)}. \quad (35)$$

### D. Probe type (1)

When  $H_{pk}^{(1)}$  takes  $H_{p1}^{(1)}$ , using Eqs. (30)-(31), we have the linear response as

$$I_{s1}^{(1)}(0, t) = \text{Re}\{\tilde{I}_{s1}(\omega_1) e^{-i\omega_1 t}\} + \text{Re}\{\tilde{I}_{s1}(\omega_{1-}) e^{-i\omega_{1-} t}\} \quad (36)$$

where  $\omega_{1-} = \omega_1 - \omega_{d1}$  is the produced difference frequency. The amplitudes of both frequency components are respectively denoted as  $\tilde{I}_{s1}(\omega_1)$  and  $\tilde{I}_{s1}(\omega_{1-})$ . The gain of the incident current  $I_{p1}$  is defined as  $G_1 = 1 + \tilde{I}_{s1}(\omega_1)/\tilde{I}_{p1}$ , and the explicit expression is

$$G_1 = 1 - \frac{M^2}{2\hbar Z_T} \frac{\rho_{11}^{(0)} \lambda_{31} \cos^2 \frac{\theta_1}{2}}{i(\omega_{31}^{(1)} - \omega_1) + \frac{1}{2}\Gamma_{31}^{(1)}} - \frac{M^2}{2\hbar Z_T} \frac{\rho_{22}^{(0)} \lambda_{31} \sin^2 \frac{\theta_1}{2}}{i(\omega_{32}^{(1)} - \omega_1) + \frac{1}{2}\Gamma_{32}^{(1)}}. \quad (37)$$

Meanwhile, the corresponding efficiency of frequency down conversion is defined as  $\eta_1 = \tilde{I}_{s1}(\omega_{1-})/\tilde{I}_{p1} \sqrt{\omega_1/\omega_{1-}}$  since  $|\eta_1|^2$  represents the photon number of frequency  $\omega_{1-}$  produced by each photon of

frequency  $\omega_1$  per unit time. Then, the explicit expression of  $\eta_1$  can be reduced to

$$\eta_1 = \frac{M^2}{2\hbar Z_T} \frac{\rho_{11}^{(0)} \sqrt{\lambda_{32}\lambda_{31}} \cos \frac{\theta_1}{2} \sin \frac{\theta_1}{2}}{i \left( \omega_{31}^{(1)} - \omega_1 \right) + \frac{1}{2}\Gamma_{31}^{(1)}} + \frac{M^2}{2\hbar Z_T} \frac{\rho_{22}^{(0)} \sqrt{\lambda_{32}\lambda_{31}} \cos \frac{\theta_1}{2} \sin \frac{\theta_1}{2}}{i \left( \omega_{32}^{(1)} - \omega_1 \right) + \frac{1}{2}\Gamma_{32}^{(1)}}. \quad (38)$$

The two resonant points of  $G_1$  and  $\eta_1$  are respectively at  $\omega_1 = \omega_{31}^{(1)}$  and  $\omega_1 = \omega_{32}^{(1)}$ . As  $\Omega_{21,1}$  is assumed larger than the decay rates, the two resonant points must be well separated. Therefore, we can determine from Eq. (37) that the transmitted signal with frequency  $\omega_1$  can only be attenuated. At both points,  $|G_1|$  ( $|\eta_1|$ ) reaches their minimum (maximum) values respectively. To obtain the optimal attenuation or conversion efficiency, we can first minimize  $\Gamma_{31}^{(1)}$  and  $\Gamma_{32}^{(1)}$  where

$$\Gamma_{31}^{(1)} = \frac{M^2}{\hbar Z_T} \left( \lambda_{31} + \lambda_{32} + \sin^2 \frac{\theta_1}{2} \lambda_{21} \right), \quad (39)$$

$$\Gamma_{32}^{(1)} = \frac{M^2}{\hbar Z_T} \left( \lambda_{31} + \lambda_{32} + \cos^2 \frac{\theta_1}{2} \lambda_{21} \right). \quad (40)$$

The dephasing rates  $\Gamma_{31}^{(1)}$  and  $\Gamma_{32}^{(1)}$  can be further reduced to

$$\Gamma_{31}^{(1)} = \frac{M^2}{\hbar Z_T} (\lambda_{31} + \lambda_{32}), \quad (41)$$

$$\Gamma_{32}^{(1)} = \frac{M^2}{\hbar Z_T} (\lambda_{31} + \lambda_{32}), \quad (42)$$

in the limit that  $\lambda_3 = \lambda_{32}/\lambda_{21} \gg 1$  and  $\lambda_2 = \lambda_{31}/\lambda_{21} \gg 1$ . We thus assume  $\lambda_3 \gg 1$  and  $\lambda_2 \gg 1$  in the following discussions of  $\eta_1$  and  $G_1$ .

We now further seek the limitation value of  $|G_1|$  when  $\omega_1 = \omega_{31}^{(1)}$ . In this case,  $G_1$  is reduced to

$$G_1 = 1 - \frac{\lambda_1}{(\lambda_1 + 1)(1 + y_1)} \frac{1}{1 + y_1^2}, \quad (43)$$

where  $\lambda_1 = \lambda_{31}/\lambda_{32}$ . Apparently, when  $\lambda_1 \gg 1$  and  $y_1 \ll 1$ , the optimal gain for attenuation can reach

$$G_1 = 0. \quad (44)$$

In the resonant driving case,  $y_1 = 1$ , and the best gain for attenuation can reach

$$G_1 = \frac{3}{4}, \quad (45)$$

under the condition  $\lambda_1 \gg 1$ . In Fig. 3(a),  $G_1$  takes Eq. (43). We have plotted  $|G_1|$  as functions of  $y_1$  when  $\lambda_1$  takes 0.2, 1, and 10, respectively. It can be easily seen that  $|G_1|$  will decrease as  $\lambda_1$  increases or  $y_1$  decreases. It is a similar case when  $\omega_1 = \omega_{32}^{(1)}$ , where the gain becomes

$$G_1 = 1 - \frac{\lambda_1}{(\lambda_1 + 1)(1 + y_1^{-1})} \frac{1}{1 + y_1^{-2}}. \quad (46)$$

The similarity can be easily found between Eqs. (43) and (46). Thus, we directly have the optimal gain for attenuation

$$G_1 = 0, \quad (47)$$

when  $\lambda_1 \gg 1$  and  $y_1^{-1} \ll 1$ . In the resonant driving case,  $y_1 = 1$ , and the optimal gain for attenuation can reach

$$G_1 = \frac{3}{4} \quad (48)$$

with the condition  $\lambda_1 \gg 1$ . The properties of  $|G_1|$  when  $G_1$  takes (46) can also be investigated through Fig. 3(a).

We now seek the limitation of  $|\eta_1|$  when  $\omega_1 = \omega_{31}^{(1)}$ . In this case,  $\eta_1$  is reduced to

$$\eta_1 = \frac{\sqrt{\lambda_1}}{(\lambda_1 + 1)(1 + y_1)} \frac{\sqrt{y_1}}{1 + y_1^2}. \quad (49)$$

It can be proved that when  $\lambda_1 = 1$  and  $y_1 = 0.36349$ , the optimal conversion efficiency reads

$$\eta_1 = 0.19529. \quad (50)$$

In the resonant driving case,  $y_1 = 1$ , and we have the optimal conversion efficiency

$$\eta_1 = \frac{1}{8}, \quad (51)$$

under the condition  $\lambda_1 = 1$ . In Fig. 3(b),  $\eta_1$  takes Eq. (49). We have plotted  $|\eta_1|$  as functions of  $y_1$  when  $\lambda_1$  takes 0.2, 1, and 10, respectively. As  $\lambda_1$  is given and  $y_1$  increases,  $|\eta_1|$  first increases to the maximum point and then fall towards zero. Given  $y_1$ , the maximum  $|\eta_1|$  emerges at  $\lambda_1 = 1$ . It is a similar case when  $\omega_1 = \omega_{32}^{(1)}$ , where the conversion efficiency becomes

$$\eta_1 = \frac{\sqrt{\lambda_1}}{(\lambda_1 + 1)(y_1^{-1} + 1)} \frac{\sqrt{y_1^{-1}}}{(1 + y_1^{-2})}. \quad (52)$$

The similarity can be easily found between Eqs. (49) and (52). Thus, the optimal conversion efficiency reads

$$\eta_1 = 0.19529, \quad (53)$$

when  $\lambda_1 = 1$  and  $y_1^{-1} = 0.36349$ . In the resonant driving case, i.e.,  $y_1 = 1$ , we have the optimal conversion efficiency

$$\eta_1 = \frac{1}{8} \quad (54)$$

also under the condition  $\lambda_1 = 1$ . The properties of  $|\eta_1|$  when  $\eta_1$  takes (52) can also be investigated through Fig. 3(b).

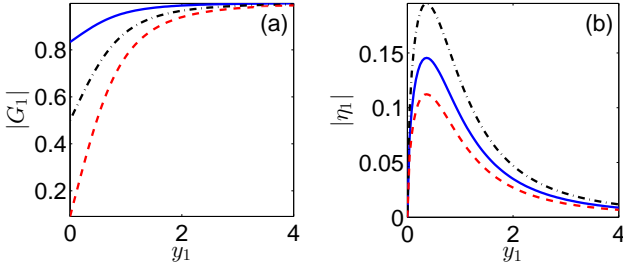


FIG. 3: (Color online) Probe type (1), driving type (1). The gain (a)  $|G_1|$  and conversion efficiency (b)  $|\eta_1|$  plotted as functions of  $y_1$ . Here, we have assumed that  $\omega_1 = \omega_{31}^{(1)}$  and  $\lambda_2, \lambda_3 \gg 1$ . In both (a) and (b),  $\lambda_1 = 0.2$  (solid blue), 1 (dash-dotted black), and 10 (dashed red), respectively.

### E. Probe type (2)

When  $H_{pk}^{(1)}$  takes  $H_{p2}^{(1)}$ , using Eqs. (32)-(33), we have the linear response as

$$I_{s1}^{(1)}(0, t) = \text{Re}\{\tilde{I}_{s1}(\omega_2)e^{-i\omega_1 t}\} + \text{Re}\{\tilde{I}_{s1}(\omega_{2+})e^{-i\omega_{2+} t}\}. \quad (55)$$

The amplitudes of both frequency components are respectively  $\tilde{I}(\omega_2)$  and  $\tilde{I}(\omega_{2+})$ . The gain of the incident current  $I_{p2}$  is defined as  $G_2 = 1 + \tilde{I}_{s1}(\omega_2)/\tilde{I}_{p2}$ , and the explicit expression is

$$G_2 = 1 - \frac{M^2}{2\hbar Z_T} \frac{\rho_{11}^{(0)} \lambda_{32} \sin^2 \frac{\theta_1}{2}}{i \left( \omega_{31}^{(1)} - \omega_{2+} \right) + \frac{1}{2} \Gamma_{31}^{(1)}} - \frac{M^2}{2\hbar Z_T} \frac{\rho_{22}^{(0)} \lambda_{32} \cos^2 \frac{\theta_1}{2}}{i \left( \omega_{32}^{(1)} - \omega_{2+} \right) + \frac{1}{2} \Gamma_{32}^{(1)}} \quad (56)$$

Meanwhile, the corresponding efficiency of frequency down conversion is defined as  $\eta_2 = \tilde{I}_{s1}(\omega_{2+})/\tilde{I}_{p2}\sqrt{\omega_2/\omega_{2+}}$  since  $|\eta_2|^2$  represents the photon number of frequency  $\omega_{2+}$  produced by each photon of frequency  $\omega_2$  per unit time. The explicit expression of  $\eta_2$  is hence

$$\eta_2 = \frac{M^2}{2\hbar Z_T} \frac{\sqrt{\lambda_{31}\lambda_{32}}\rho_{11}^{(0)} \sin \frac{\theta_1}{2} \cos \frac{\theta_1}{2}}{i \left( \omega_{31}^{(1)} - \omega_{2+} \right) + \frac{1}{2} \Gamma_{31}^{(1)}} - \frac{M^2}{2\hbar Z_T} \frac{\sqrt{\lambda_{31}\lambda_{32}}\rho_{22}^{(0)} \sin \frac{\theta_1}{2} \cos \frac{\theta_1}{2}}{i \left( \omega_{32}^{(1)} - \omega_{2+} \right) + \frac{1}{2} \Gamma_{32}^{(1)}}. \quad (57)$$

The two resonant points of  $G_2$  and  $\eta_2$  are respectively at  $\omega_{2+} = \omega_{31}^{(1)}$  and  $\omega_{2+} = \omega_{32}^{(1)}$ . As we have assumed a sufficiently large  $\Omega_{21,1}$ , the two resonant points must be well separated. Therefore, we can know from Eq. (56) that the transmitted signal with frequency  $\omega_2$  can only be attenuated. At both points,  $|G_2|$  ( $|\eta_2|$ ) reaches their minimum (maximum) values respectively. As in probe type (1), we should also assume  $\lambda_3 \gg 1$  and  $\lambda_2 \gg 1$  in

the following discussions for achieving optimal  $|G_2|$  and  $|\eta_2|$ .

We now further seek the limitation value of  $|G_2|$  when  $\omega_{2+} = \omega_{31}^{(1)}$ . In this case,  $G_2$  is reduced to

$$G_2 = 1 - \frac{y_1}{(\lambda_1 + 1)(1 + y_1)} \frac{1}{1 + y_1^2}. \quad (58)$$

It can be proved that when  $\lambda_1 \ll 1$ , and  $y_1 = 0.65730$ , we can achieve the optimal gain for attenuation, that is,

$$G_2 = 0.72305. \quad (59)$$

In the resonant driving case, i.e.,  $y_1 = 1$ , the optimal gain for attenuation can reach

$$G_2 = \frac{3}{4}, \quad (60)$$

under the condition  $\lambda_1 \ll 1$ . In Fig 4(a),  $G_2$  takes Eq. (58). We have plotted  $|G_2|$  as functions of  $y_1$  when  $\lambda_1$  takes 0.2, 1, and 10, respectively. When  $y_1$  increases,  $|G_2|$  will first decrease until meeting the minimum point and then switch to increase. As  $\lambda_1$  increases,  $|G_2|$  will also increase. It is a similar case when  $\omega_{2+} = \omega_{32}^{(1)}$ , where the gain becomes

$$G_2 = 1 - \frac{y_1^{-1}}{(\lambda_1 + 1)(1 + y_1^{-1})} \frac{1}{1 + y_1^{-2}}. \quad (61)$$

The similarity can be easily found between Eqs. (58) and (61). Thus we can obtain that when  $\lambda_1 \ll 1$  and  $y_1^{-1} = 0.65730$ , the optimal gain for attenuation reads

$$G_2 = 0.72305. \quad (62)$$

In the resonant driving case, i.e.,  $y_1 = 1$ , we have the optimal gain for attenuation

$$G_2 = \frac{3}{4}, \quad (63)$$

under the condition  $\lambda_1 \ll 1$ . When  $G_2$  takes Eq. (61),  $|G_2|$  can also be investigated through Fig 4(a).

We now seek the limitation of  $|\eta_2|$  when  $\omega_{2+} = \omega_{31}^{(1)}$ . In this case,  $\eta_2$  is reduced to

$$\eta_2 = \frac{\sqrt{\lambda_1}}{(\lambda_1 + 1)(1 + y_1)} \frac{\sqrt{y_1}}{(1 + y_1^2)}. \quad (64)$$

We find that Eqs. (64) and (49) are exactly of the same form. We thus directly give that when  $\lambda_1 = 1$  and  $y_1 = 0.36349$ , the optimal conversion efficiency reads

$$\eta_2 = 0.19529. \quad (65)$$

In the resonant driving case,  $y_1 = 1$ , and the optimal conversion efficiency reads

$$\eta_2 = \frac{1}{8}, \quad (66)$$



when  $\lambda_1 = 1$ . It is a similar case when  $\omega_{2+} = \omega_{32}^{(1)}$ , where the conversion efficiency becomes

$$\eta_2 = -\frac{\sqrt{\lambda_1}}{(\lambda_1 + 1)(1 + y_1^{-1})} \frac{\sqrt{y_1^{-1}}}{1 + y_1^{-2}}. \quad (67)$$

The similarity can be easily found between Eqs. (64) and (67). We hence obtain that when  $\lambda_1 = 1$  and  $y_1^{-1} = 0.36349$ , the optimal conversion efficiency reads

$$\eta_2 = 0.19529. \quad (68)$$

In the resonant driving case,  $y_1 = 1$ , and the optimal conversion efficiency reads

$$\eta_2 = \frac{1}{8}, \quad (69)$$

when  $\lambda_1 = 1$ . For completeness, we also plot Fig. 4(b) for  $|\eta_2|$ . Whether  $\eta_2$  takes Eq. (64) or (67), the behaviours of  $|\eta_2|$  can be investigated through Fig. 4(b).

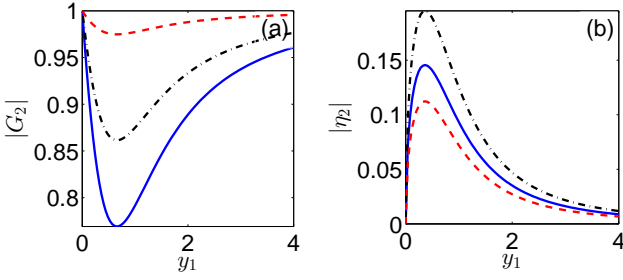


FIG. 4: (Color online) Probe type (2), driving type (1). The gain (a)  $|G_2|$  and conversion efficiency (b)  $|\eta_2|$  plotted as functions of  $y_1$ . Here, we have assumed that  $\omega_{2+} = \omega_{31}^{(1)}$  and  $\lambda_2, \lambda_3 \gg 1$ . In both (a) and (b),  $\lambda_1 = 0.2$  (solid blue), 1 (dash-dotted black), and 10 (dashed red), respectively.

#### IV. MICROWAVE ATTENUATION AND FREQUENCY CONVERSIONS FOR DRIVING TYPE (2)

##### A. Hamiltonian reduction

In the driving type (2), the Hamiltonian  $H_R^{(2)}(t)$  can be given as

$$H_R^{(2)}(t) = \hbar \Omega_{32,2} \exp(-i\omega_{d2}t) \sigma_{32} + \text{H.c.} \quad (70)$$

with  $\Omega_{32,2} = -M I_{32} \tilde{I}_{d2}/2$ . The incident driving current is assumed as  $I_{d2}(x, t) = \text{Re}[\tilde{I}_{d2} e^{-i\omega_{d2}(t-x/v)}]$  with the phase velocity  $v$ . We assume that  $\Omega_{32,2}$  is a real number without loss of generality.

Corresponding to the Hamiltonian in Eq. (70), the Hamiltonian  $H_{pk}^{(2)}(t)$  with  $k = 3$  or 4 are respectively

$$H_{p3}^{(1)}(t) = -M \hat{I}_{p3}(0, t), \quad (71)$$

$$H_{p4}^{(1)}(t) = -M \hat{I}_{p4}(0, t), \quad (72)$$

without RWA. The Hamiltonian in Eq. (1) with  $H_R^{(2)}(t)$  in Eq. (70) and  $H_{p3}^{(2)}(t)$  in Eq. (71) describes the frequency down conversion as shown in the up panel of Fig. 1(c). However, the Hamiltonian  $H_{p4}^{(2)}(t)$  can be written as for that the signal field is applied to the energy levels  $|1\rangle$  and  $|2\rangle$ . That is, the Hamiltonian in Eq. (1) with  $H_R^{(2)}(t)$  in Eq. (70) and  $H_{p4}^{(2)}(t)$  in Eq. (72) describes the frequency up conversion as shown in the down panel of Fig. 1(c). The incident signal currents are assumed as  $I_{pk}(x, t) = \text{Re}[\tilde{I}_{pk} e^{-i\omega_k(t-x/v)}]$  with  $k = 3$  or  $k = 4$ .

To remove the time dependence of  $H^{(2)}$ , we now use a unitary transformation  $U_d^{(2)} = \exp(-i\omega_{d2}t\sigma_{33})$ . Then at a frame rotating, we get an effective Hamiltonian

$$\begin{aligned} H_{\text{eff}}^{(2)} = & \hbar \omega_{21} \sigma_{22} + \hbar (\omega_{21} + \Delta_{32,2}) \sigma_{33} + \hbar \Omega_{32,2} (\sigma_{32} + \sigma_{23}) \\ & - M \hat{I}^{(2)}(t) (I_L(0, t) + I_R(0, t)) \\ & - M \hat{I}^{(2)}(t) I_{pk}(0, t), \end{aligned} \quad (73)$$

with driving detuning  $\Delta_{32,2} = \omega_{32} - \omega_{d2}$  and the transformed loop current  $\hat{I}^{(2)}(t) = U_d^{(2)\dagger} \hat{I} U_d^{(2)}$ . Furthermore, we think driving strengths  $\Omega_{mn,l}$  are strong enough compared to the decay rates of the flux qubit circuit. Then, we should work in the eigen basis of the first three terms of Eq. (73). Thus, we apply to  $H_{\text{eff}}^{(2)}$  a unitary transformation  $U_r^{(2)} = \exp(-i\theta_2(-i\sigma_{32} + i\sigma_{23})/2)$  with  $\tan \theta_2 = 2\Omega_{32,2}/\Delta_{32,2}$ , yielding

$$\bar{H}_{\text{eff}}^{(2)} = H_S^{(2)} + \bar{H}_{pk}^{(2)} + H_T^{(2)}, \quad (74)$$

where

$$H_S^{(2)} = \hbar \omega_{21} \sigma_{22} + \hbar \omega_{31} \sigma_{33}, \quad (75)$$

$$\bar{H}_{pk}^{(2)} = -M \bar{I}^{(2)}(t) I_{pk}(0, t), \quad (76)$$

$$H_T^{(2)} = -M \bar{I}^{(2)}(t) (I_L(0, t) + I_R(0, t)). \quad (77)$$

Note that  $\bar{I}^{(2)}(t) = U_r^{(2)\dagger} \hat{I}^{(2)}(t) U_r^{(2)}$  is another transformed loop current and its matrix elements have been listed in Appendix. B. Here,  $H_S^{(2)}$  is treated as the system Hamiltonian originating from the first three terms in Eq. (73). In Eq. (75), the eigen frequencies are respectively

$$\omega_{21}^{(2)} = \omega_{21} + \frac{1}{2} \left( \Delta_{32,2} - \sqrt{4\Omega_{32,2}^2 + \Delta_{32,2}^2} \right), \quad (78)$$

$$\omega_{31}^{(2)} = \omega_{21} + \frac{1}{2} \left( \Delta_{32,2} + \sqrt{4\Omega_{32,2}^2 + \Delta_{32,2}^2} \right). \quad (79)$$

The Hamiltonian  $\bar{H}_{pk}^{(2)}$  is a small quantity compared to  $H_S^{(2)}$  and hence will be treated as the perturbation to the system Hamiltonian. Besides,  $H_T^{(2)}$  determines the dissipation of the system into the 1D open space. Without fast oscillating terms neglected,  $\bar{H}_{pk}^{(2)}$  can be further reduced to

$$\bar{H}_{p3} = \hbar \varepsilon_{21,3} e^{-i\omega_{3-}t} \sigma_{21} + \hbar \varepsilon_{31,3} e^{-i\omega_{3-}t} \sigma_{31} + \text{h.c.}, \quad (80)$$

$$\bar{H}_{p4} = \hbar \varepsilon_{21,4} e^{-i\omega_{4-}t} \sigma_{21} + \hbar \varepsilon_{31,4} e^{-i\omega_{4-}t} \sigma_{31} + \text{h.c.}, \quad (81)$$



where  $\omega_{3-} = \omega_3 - \omega_{d2}$  is the produced difference frequency, and the coupling energy parameters are

$$\hbar\varepsilon_{21,3} = \frac{1}{2}M \sin \frac{\theta_2}{2} \tilde{I}_{p3} I_{31}, \quad (82)$$

$$\hbar\varepsilon_{31,3} = -\frac{1}{2}M \cos \frac{\theta_2}{2} \tilde{I}_{p3} I_{31}, \quad (83)$$

$$\hbar\varepsilon_{21,4} = -\frac{1}{2}M \cos \frac{\theta_2}{2} \tilde{I}_{p4} I_{21}, \quad (84)$$

$$\hbar\varepsilon_{31,4} = -\frac{1}{2}M \sin \frac{\theta_2}{2} \tilde{I}_{p4} I_{21}. \quad (85)$$

### B. Dynamics of the system and its solutions

Using the detailed parameters of  $\bar{I}^{(2)}(t)$  in Appendix. B, we can derive that the reduced density matrix  $\chi$  of the system is governed by the following master equation [55]

$$\frac{\partial \chi}{\partial t} = \frac{1}{i\hbar} [H_S^{(2)} + \bar{H}_{pk}^{(2)}, \chi] + \mathcal{L}[\chi]. \quad (86)$$

We must mention we work in the picture defined by unitary transformations  $U_d^{(1)}$  and  $U_r^{(1)}$ . The dissipation of the system is described via the Lindblad term

$$\begin{aligned} \mathcal{L}[\chi] = & \sum_m \left( \sum_{k \neq m} \gamma_{km}^{(2)} \chi_{kk} - \sum_{k \neq m} \gamma_{mk}^{(2)} \chi_{mm} \right) \sigma_{mm} \\ & - \sum_{m \neq n} \frac{1}{2} \Gamma_{mn}^{(2)} \chi_{mn} \sigma_{mn}. \end{aligned} \quad (87)$$

Here,  $\chi_{mn} \equiv \chi_{mn}(t)$  are matrix elements of the reduced density operator  $\chi(t)$ . The relaxation and dephasing rates can be calculated as  $\gamma_{mn}^{(2)} = \frac{M^2}{\hbar Z_T} K_{mn}^{(2)}$  and  $\Gamma_{mn}^{(2)} = \frac{M^2}{\hbar Z_T} \left( \sum_{k \neq m} K_{mk}^{(2)} + \sum_{k \neq n} K_{nk}^{(2)} + K_{\phi mn}^{(2)} \right)$  from hypotheses (1), (2), and (4) in Sec. II. The explicit expressions of  $K_{mn}^{(2)}$  and  $K_{\phi mn}^{(2)}$  are given in Appendix. B.

Then we seek the solutions of Eq. (86) in the form of a power series expansion in the magnitude of  $\bar{H}_{pk}^{(2)}$ , that is, a solution of the form

$$\chi(t) = \chi^{(0)} + \chi^{(1)}(t) + \cdots + \chi^{(r)}(t) + \cdots, \quad (88)$$

for the reduced density matrix  $\chi$  of the three-level system. Here,  $\chi^{(0)}$  is the steady state solution when no signal field is applied to the system. However the  $r$ th-order reduced density matrix  $\chi^{(r)}(t)$  is proportional to  $r$ th order of  $\bar{H}_{pk}^{(2)}$ .

In the first order approximation, we have

$$\frac{\partial \chi^{(0)}}{\partial t} = \frac{1}{i\hbar} [H_S^{(2)}, \chi^{(0)}] + \mathcal{L}[\chi^{(0)}], \quad (89)$$

$$\frac{\partial \chi^{(1)}}{\partial t} = \frac{1}{i\hbar} [H_S^{(2)}, \chi^{(1)}] + \frac{1}{i\hbar} [\bar{H}_{pk}^{(2)}, \chi^{(0)}] + \mathcal{L}[\chi^{(1)}]. \quad (90)$$

The solutions of Eq. (89) is

$$\chi_{11}^{(0)} = 1. \quad (91)$$

And the other terms of  $\chi^{(0)}$  are all zeros. Having obtained  $\chi^{(0)}$ , we can future solve Eq. (90). When  $\bar{H}_{pk}^{(2)}$  takes  $\bar{H}_{p3}^{(2)}$ , we have the nonzero matrix elements of  $\chi^{(1)}$  as follows,

$$\chi_{21}^{(1)} = \chi_{12}^{(1)*} = -\frac{i\varepsilon_{21,3} e^{-i\omega_{3-}t}}{i(\omega_{21}^{(2)} - \omega_{3-}) + \frac{1}{2}\Gamma_{21}^{(2)}}, \quad (92)$$

$$\chi_{31}^{(1)} = \chi_{13}^{(1)*} = -\frac{i\varepsilon_{31,3} e^{-i\omega_{3-}t}}{i(\omega_{31}^{(2)} - \omega_{3-}) + \frac{1}{2}\Gamma_{31}^{(2)}}. \quad (93)$$

When  $\bar{H}_{pk}^{(2)}$  takes  $\bar{H}_{p4}^{(2)}$ , we have the nonzero matrix elements of  $\chi^{(1)}$  as follows,

$$\chi_{21}^{(1)} = \chi_{12}^{(1)*} = -\frac{i\varepsilon_{21,4} e^{-i\omega_4 t}}{i(\omega_{21}^{(2)} - \omega_4) + \frac{1}{2}\Gamma_{21}^{(2)}}, \quad (94)$$

$$\chi_{31}^{(1)} = \chi_{13}^{(1)*} = -\frac{i\varepsilon_{31,4} e^{-i\omega_4 t}}{i(\omega_{31}^{(2)} - \omega_4) + \frac{1}{2}\Gamma_{31}^{(2)}}. \quad (95)$$

### C. Scattered current

The scattered current at  $x = 0$ , similarly to driving type (1), can be represented by

$$I_{s2}(0, t) = -\frac{iM}{2Z_T} \sum_{mnk} \delta_{mnk}^{(2)} \bar{I}_{mnk}^{(2)} e^{i\nu_{mnk}^{(2)} t} \chi_{nm}, \quad (96)$$

with  $\delta_{mnk}^{(2)} = \omega_{mn}^{(2)} + \nu_{mnk}^{(2)}$ . Here, we have assumed that the matrix element of  $\bar{I}^{(2)}(t)$  is of the form  $\bar{I}_{mn}^{(2)}(t) = \sum_k \bar{I}_{mnk}^{(2)} e^{i\nu_{mnk}^{(2)} t}$ . We hereby also expand the scattered current as  $I_{s2} = \sum_{r=0}^{\infty} I_{s2}^{(r)}$ , where  $I_{s2}^{(r)}$  is in the  $r$ th order of  $\bar{H}_{pk}^{(2)}$ . In this paper, we only care about the linear response of  $\bar{H}_{pk}^{(2)}$ , that is,

$$I_{s2}^{(1)}(0, t) = -\frac{iM}{2Z_T} \sum_{mnk} \delta_{mnk}^{(2)} \bar{I}_{mnk}^{(2)} e^{i\nu_{mnk}^{(2)} t} \chi_{nm}^{(1)}. \quad (97)$$

### D. Probe type (3)

When  $H_{pk}^{(2)}$  takes  $H_{p2}^{(2)}$ , using Eqs. (94)-(95), we have the linear response as

$$I_{s2}^{(1)}(0, t) = \text{Re}\{\tilde{I}_{s2}(\omega_3) e^{-i\omega_3 t}\} + \text{Re}\{\tilde{I}_{s2}(\omega_{3-}) e^{-i\omega_{3-} t}\} \quad (98)$$

where  $\omega_{3-} = \omega_3 - \omega_{d2}$  is the produced difference frequency. The amplitudes of both frequency components are respectively  $\tilde{I}_{s2}(\omega_3)$  and  $\tilde{I}_{s2}(\omega_{3-})$ . The gain of the

incident current  $I_{p3}$  is defined as  $G_3 = 1 + \tilde{I}_{s2}(\omega_3)/\tilde{I}_{p3}$ , and the explicit expression is

$$G_3 = 1 - \frac{M^2}{2\hbar Z_T} \frac{\lambda_{31} \sin^2 \frac{\theta_2}{2}}{i \left( \omega_{21}^{(2)} - \omega_{3-} \right) + \frac{1}{2} \Gamma_{21}^{(2)}} - \frac{M^2}{2\hbar Z_T} \frac{\lambda_{31} \cos^2 \frac{\theta_2}{2}}{i \left( \omega_{31}^{(2)} - \omega_{3-} \right) + \frac{1}{2} \Gamma_{31}^{(2)}}. \quad (99)$$

Meanwhile, the corresponding efficiency of frequency down conversion is defined as  $\eta_3 = \tilde{I}_{s2}(\omega_{3-})/\tilde{I}_{p3}\sqrt{\omega_3/\omega_{3-}}$  since  $|\eta_3|^2$  represents the photon number of frequency  $\omega_{3-}$  produced by each photon of frequency  $\omega_3$  per unit time. The explicit expression of  $\eta_3$  is hence

$$\eta_3 = \frac{M^2}{2\hbar Z_T} \frac{\sqrt{\lambda_{21}\lambda_{31}} \sin \frac{\theta_2}{2} \cos \frac{\theta_2}{2}}{i \left( \omega_{21}^{(2)} - \omega_{3-} \right) + \frac{1}{2} \Gamma_{21}^{(2)}} - \frac{M^2}{2\hbar Z_T} \frac{\sqrt{\lambda_{21}\lambda_{31}} \sin \frac{\theta_2}{2} \cos \frac{\theta_2}{2}}{i \left( \omega_{31}^{(2)} - \omega_{3-} \right) + \frac{1}{2} \Gamma_{31}^{(2)}}. \quad (100)$$

The two resonant points of  $G_3$  and  $\eta_3$  are respectively at  $\omega_{3-} = \omega_{21}^{(2)}$  and  $\omega_{3-} = \omega_{31}^{(2)}$ . As we have assumed a sufficiently large  $\Omega_{32,2}$ , the two resonant points must be well separated. Therefore, we can determine from Eq. (99) that the transmitted signal with frequency  $\omega_3$  can only be attenuated. At both points,  $|G_3|$  ( $|\eta_3|$ ) reaches their minimum (maximum) values respectively. To obtain the optimal attenuation or conversion efficiency, we can first minimize  $\Gamma_{21}^{(2)}$  and  $\Gamma_{31}^{(2)}$  where

$$\Gamma_{21}^{(2)} = \frac{M^2}{\hbar Z_T} \left[ \lambda_{21} \cos^2 \frac{\theta_2}{2} + (\lambda_{31} + \lambda_{32}) \sin^2 \frac{\theta_2}{2} \right], \quad (101)$$

$$\Gamma_{31}^{(2)} = \frac{M^2}{\hbar Z_T} \left[ \lambda_{21} \sin^2 \frac{\theta_2}{2} + (\lambda_{31} + \lambda_{32}) \cos^2 \frac{\theta_2}{2} \right]. \quad (102)$$

The dephasing rates  $\Gamma_{21}^{(2)}$  and  $\Gamma_{31}^{(2)}$  can be further reduced to

$$\Gamma_{21}^{(2)} = \frac{M^2}{\hbar Z_T} \left( \lambda_{21} \cos^2 \frac{\theta_2}{2} + \lambda_{31} \sin^2 \frac{\theta_2}{2} \right), \quad (103)$$

$$\Gamma_{31}^{(2)} = \frac{M^2}{\hbar Z_T} \left( \lambda_{21} \sin^2 \frac{\theta_2}{2} + \lambda_{31} \cos^2 \frac{\theta_2}{2} \right). \quad (104)$$

in the limit that  $\lambda_1 = \lambda_{31}/\lambda_{32} \gg 1$  and  $\lambda_3 = \lambda_{32}/\lambda_{21} \ll 1$ . We thus assume  $\lambda_1 \gg 1$  and  $\lambda_3 \ll 1$  in the following discussions of  $\eta_3$  and  $G_3$ .

We now further seek the limitation value of  $|G_3|$  when  $\omega_{3-} = \omega_{21}^{(2)}$ . In this case,  $G_3$  is reduced to

$$G_3 = 1 - \frac{\lambda_2 y_2}{1 + \lambda_2 y_2}, \quad (105)$$

with  $y_2 = \tan^2(\theta_2/2)$ . Apparently, when  $\lambda_2 y_2 \gg 1$ , the optimal gain for attenuation reads

$$G_3 = 0. \quad (106)$$

In the resonant driving case,  $y_2 = 1$ , and the optimal attenuation  $G_3 = 0$  is also achievable with  $\lambda_2 \gg 1$ . In Fig. 5(a),  $G_3$  takes Eq. (105). We have plotted  $|G_3|$  as a function of  $\lambda_2 y_2$ . When  $\lambda_2 y_2$  increases,  $|G_3|$  also shows decrease towards zero. It is a similar case when  $\omega_{3-} = \omega_{31}^{(2)}$ , where the gain becomes

$$G_3 = 1 - \frac{\lambda_2 y_2^{-1}}{1 + \lambda_2 y_2^{-1}}. \quad (107)$$

The similarity can be easily found between Eqs. (105) and (107). Thus, the optimal gain for attenuation reads

$$G_3 = 0. \quad (108)$$

when the condition  $\lambda_2 y_2^{-1} \gg 1$  is satisfied. In the resonant driving case,  $y_2 = 1$ , and the optimal gain for attenuation  $G_3 = 0$  is also achieved with  $\lambda_2 \gg 1$ . When  $G_3$  takes Eq. (107), the properties of  $|G_3|$  can also be investigated through Fig. 5(a).

We now seek the limitation of  $|\eta_3|$  when  $\omega_{3-} = \omega_{21}^{(2)}$ . In this case,  $\eta_3$  is reduced to

$$\eta_3 = \frac{\sqrt{\lambda_2 y_2}}{1 + \lambda_2 y_2}. \quad (109)$$

When  $\lambda_2 y_2 = 1$ , the optimal conversion efficiency reads

$$\eta_3 = \frac{1}{2}. \quad (110)$$

In the resonant driving case,  $y_2 = 1$ , and the optimal conversion efficiency  $\eta_3 = 1/2$  is also achievable when  $\lambda_2 = 1$ . In Fig. 5(b),  $\eta_3$  takes Eq. (109). We have plotted  $|\eta_3|$  as a function of  $\lambda_2 y_2$ . When  $\lambda_2 y_2$  increases, we find that  $|\eta_3|$  first increases to the optimal point and then falls towards zero. It is a similar case when  $\omega_{3-} = \omega_{31}^{(2)}$ , where the conversion efficiency reads

$$\eta_3 = -\frac{\sqrt{\lambda_2 y_2^{-1}}}{1 + \lambda_2 y_2^{-1}}. \quad (111)$$

The similarity can be easily found between Eqs. (111) and (109). When  $\lambda_2 y_2^{-1} = 1$ , we have the optimal conversion efficiency

$$\eta_3 = -\frac{1}{2}. \quad (112)$$

In the resonant driving case,  $y_2 = 1$ , and the optimal conversion efficiency  $\eta_3 = -1/2$  is also accessible with  $\lambda_2 = 1$ . When  $\eta_3$  takes Eq. (111), the property of  $|\eta_3|$  can be similarly investigated through Fig. 5(b).

### E. Probe type (4)

When  $H_{pk}^{(2)}$  takes  $H_{p4}^{(2)}$ , using Eqs. (94)-(95), we have the linear response as

$$I_{s2}^{(1)}(0, t) = \text{Re}\{\tilde{I}_{s2}(\omega_4)e^{-i\omega_4 t}\} + \text{Re}\{\tilde{I}_{s2}(\omega_{4+})e^{-i\omega_{4+} t}\}. \quad (113)$$

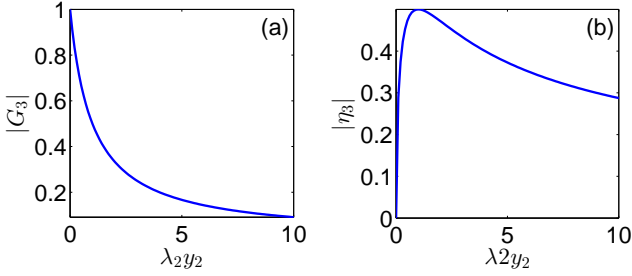


FIG. 5: (Color online) Probe type (3), driving type (2). The gain (a)  $|G_3|$  and conversion efficiency (b)  $|\eta_3|$  plotted as functions of  $\lambda_2 y_2$ . Here, we have assumed that  $\omega_{3-} = \omega_{21}^{(2)}$ ,  $\lambda_1 \gg 1$ , and  $\lambda_3 \ll 1$ .

The amplitudes of both frequency components are respectively  $\tilde{I}(\omega_4)$  and  $\tilde{I}(\omega_{4+})$ . The gain of the incident current  $I_{p4}$  is defined as  $G_4 = 1 + \tilde{I}_{s2}(\omega_4)/\tilde{I}_{p4}$ , and the explicit expression is

$$G_4 = 1 - \frac{M^2}{2\hbar Z_T} \frac{\lambda_{21} \cos^2 \frac{\theta_2}{2}}{i(\omega_{21}^{(2)} - \omega_4) + \frac{1}{2}\Gamma_{21}^{(2)}} - \frac{M^2}{2\hbar Z_T} \frac{\lambda_{21} \sin^2 \frac{\theta_2}{2}}{i(\omega_{31}^{(2)} - \omega_4) + \frac{1}{2}\Gamma_{31}^{(2)}} \quad (114)$$

Meanwhile, the corresponding efficiency of frequency down conversion is defined as  $\eta_4 = \tilde{I}(\omega_{4+})/\tilde{I}_{p4}\sqrt{\omega_4/\omega_{4+}}$  since  $|\eta_4|^2$  represents the photon number of frequency  $\omega_{4+}$  produced by each photon of frequency  $\omega_4$  per unit time. The explicit expression of  $\eta_4$  is hence

$$\eta_4 = \frac{M^2}{2\hbar Z_T} \frac{\sqrt{\lambda_{21}\lambda_{31}} \sin \frac{\theta_2}{2} \cos \frac{\theta_2}{2}}{i(\omega_{21}^{(2)} - \omega_4) + \frac{1}{2}\Gamma_{21}^{(2)}} - \frac{M^2}{2\hbar Z_T} \frac{\sqrt{\lambda_{21}\lambda_{31}} \sin \frac{\theta_2}{2} \cos \frac{\theta_2}{2}}{i(\omega_{31}^{(2)} - \omega_4) + \frac{1}{2}\Gamma_{31}^{(2)}}. \quad (115)$$

The two resonant points of  $G_4$  and  $\eta_4$  are respectively at  $\omega_{4+} = \omega_{21}^{(2)}$  and  $\omega_{4+} = \omega_{31}^{(2)}$ . As we have assumed a sufficiently large  $\Omega_{32,2}$ , the two points must be well separated. Therefore, we can determine from Eq. (114) that the transmitted signal with frequency  $\omega_4$  can only be attenuated. At both points,  $|G_4|$  ( $|\eta_4|$ ) reaches their minimum (maximum) values respectively. In the following discussions, we will similarly assume  $\lambda_1 \gg 1$  and  $\lambda_3 \ll 1$  just as in probe type (3).

We now further seek the limitation value of  $|G_4|$  when  $\omega_{4+} = \omega_{21}^{(2)}$ . In this case,  $G_4$  is hence reduced to

$$G_4 = 1 - \frac{1}{1 + \lambda_2 y_2}. \quad (116)$$

When  $\lambda_2 y_2 \ll 1$ , we have the optimal gain for attenuation reading

$$G_4 = 0. \quad (117)$$

In the resonant driving case,  $y_2 = 1$ , and the optimal gain for attenuation  $G_4 = 0$  is also achievable when  $\lambda_2 \ll 1$ . In Fig. 6(a),  $G_4$  takes 114. We have plotted  $|G_4|$  as the function of  $\lambda_2 y_2$ . When  $\lambda_2 y_2$  increase,  $|G_4|$  exhibits increase towards one. It is a similar case when  $\omega_{4+} = \omega_{31}^{(2)}$ , where the gain becomes

$$G_4 = 1 - \frac{1}{1 + \lambda_2 y_2^{-1}}. \quad (118)$$

The similarity can be easily seen between Eqs. (118) and (116). Thus when  $\lambda_2 y_2^{-1} \ll 1$ , the optimal gain attenuation reads

$$G_4 = 0. \quad (119)$$

In the resonant driving case,  $y_2 = 1$ , and the optimal attenuation is also  $G_4 = 0$  with  $\lambda_2 \ll 1$ . When  $G_4$  takes Eq. (118), the behaviours of  $|G_4|$  can be similarly explained through Fig. 6(a).

We now seek the limitation of  $|\eta_4|$  when  $\omega_{4+} = \omega_{21}^{(2)}$ . In this case, the conversion efficiency  $\eta_4$  is reduced to

$$\eta_4 = \frac{\sqrt{\lambda_2 y_2}}{1 + \lambda_2 y_2}. \quad (120)$$

Apparently, Eqs. (120) and (109) are of the same form. We hence directly have that when  $\lambda_2 y_2 = 1$ , the optimal conversion efficiency reads

$$\eta_4 = \frac{1}{2}. \quad (121)$$

In the resonant driving case,  $y_2 = 1$ , and the optimal conversion efficiency is also  $\eta_4 = 1/2$  with  $\lambda_2 = 1$ . It is a similar case when  $\omega_{4+} = \omega_{31}^{(1)}$ , where

$$\eta_4 = -\frac{\sqrt{\lambda_2 y_2^{-1}}}{1 + \lambda_2 y_2^{-1}}. \quad (122)$$

When  $\lambda_2 y_2^{-1} = 1$ , the optimal conversion efficiency reads

$$\eta_4 = -\frac{1}{2}. \quad (123)$$

In the resonant driving case,  $y_2 = 1$ , and the optimal conversion efficiency is also  $\eta_4 = -1/2$  with  $\lambda_2 = 1$ . For completeness, we also plot Fig. 6(b) for  $|\eta_4|$ . Whether  $\eta_4$  takes Eq. (120) or (122), the behaviours of  $|\eta_4|$  can be investigated through Fig. 6(b).

## V. MICROWAVE AMPLIFICATION, ATTENUATION, AND FREQUENCY CONVERSIONS IN THE DRIVING TYPE (3)

According to the analysis on the frequency conversion and the properties of the output signal field in both driving types (1) and (2). We find that the signal fields can

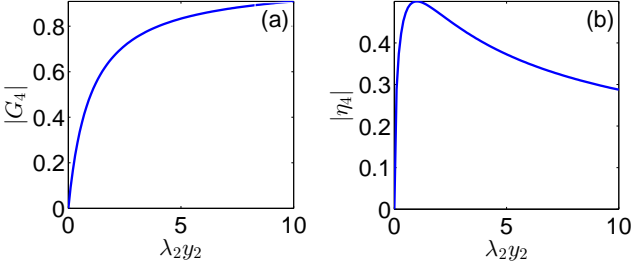


FIG. 6: (Color online) Probe type (4), driving type (2). The gain (a)  $|G_4|$  and conversion efficiency (b)  $|\eta_4|$  plotted as functions of  $\lambda_2 y_2$ . Here, we have assumed that  $\omega_4 = \omega_{21}^{(2)}$ ,  $\lambda_1 \gg 1$ , and  $\lambda_3 \ll 1$ .

only be attenuated and not be amplified in both cases. However the frequency conversion can be realized. We now study the frequency conversion and the amplification (or attenuation) of incident signal field for the driving type (3), in which the energy levels  $|1\rangle$  and  $|3\rangle$  are driven by the strong pump field, and the signal field is used to couple either the energy levels  $|1\rangle$  and  $|2\rangle$  or the energy levels  $|2\rangle$  and  $|3\rangle$ . In this driving case, we find that the incident signal field can be amplified. The detailed analysis is given below.

#### A. Hamiltonian reduction

In the driving type (3), the Hamiltonian  $H_R^{(3)}(t)$  can be given as

$$H_R^{(3)}(t) = \hbar \Omega_{31,3} \exp(-i\omega_{d3}t) \sigma_{31} + \text{H.c.} \quad (124)$$

with  $\Omega_{31,3} = -MI_{31}\tilde{I}_{d3}/2$ . The incident driving current is assumed as  $I_{d3}(x, t) = \text{Re}[\tilde{I}_{d3}e^{-i\omega_{d3}(t-x/v)}]$  with the phase velocity  $v$ . The strength  $\Omega_{31,3}$  is assumed as a real number without loss of generality.

Corresponding to the Hamiltonian in Eq. (124), the Hamiltonian  $H_{pk}^{(3)}(t)$  with  $k = 5$  or  $6$  are respectively

$$H_{p5}^{(1)}(t) = -M\hat{I}_{p5}(0, t), \quad (125)$$

$$H_{p6}^{(1)}(t) = -M\hat{I}_{p6}(0, t), \quad (126)$$

without RWA. The Hamiltonian in Eq. (1) with  $H_R^{(3)}(t)$  in Eq. (124) and  $H_{p5}^{(3)}(t)$  in Eq. (125) describes the frequency up conversion as shown in the up panel of Fig. 1(d). However, the Hamiltonian  $H_{p6}^{(3)}(t)$  can be written as for that the signal field is applied to the energy levels  $|2\rangle$  and  $|3\rangle$ . That is, the Hamiltonian in Eq. (1) with  $H_R^{(3)}(t)$  in Eq. (70) and  $H_{p4}^{(2)}(t)$  in Eq. (126) describes the frequency down conversion as shown in the down panel of Fig. 1(c). The incident signal currents are assumed as  $I_{pk}(x, t) = \text{Re}[\tilde{I}_{pk}e^{-i\omega_k(t-x/v)}]$  with  $k = 5$  or  $k = 6$ .

To remove the time dependence of  $H^{(3)}$ , we now use a unitary transformation  $U_d^{(3)} = \exp(-i\omega_{d3}t\sigma_{33})$ . Then at a frame rotating, we get an effective Hamiltonian

$$\begin{aligned} H_{\text{eff}}^{(3)} = & \hbar\omega_{21}\sigma_{22} + \hbar\Delta_{31,3}\sigma_{33} + \hbar\Omega_{31,3}(\sigma_{31} + \sigma_{13}) \\ & - M\hat{I}^{(3)}(t)(I_L(0, t) + I_R(0, t)) \\ & - M\hat{I}^{(3)}(t)I_{pk}(0, t), \end{aligned} \quad (127)$$

with driving detuning  $\Delta_{31,3} = \omega_{31} - \omega_{d3}$  and loop current  $\hat{I}^{(3)}(t) = U_d^{(3)\dagger}\hat{I}U_d^{(3)}$ . Furthermore, we think driving strengths  $\Omega_{mn,l}$  are strong enough compared to the decay rates of the flux qubit circuit. Then, we should work in the eigen basis of the first three terms of Eq. (127). Thus, we apply to  $H_{\text{eff}}^{(3)}$  a unitary transformation  $U_r^{(3)} = \exp(-i\theta_3(-i\sigma_{31} + i\sigma_{13})/2)$  with  $\tan\theta_3 = 2\Omega_{31,3}/\Delta_{31,3}$ , yielding

$$\bar{H}_{\text{eff}}^{(3)} = H_S^{(3)} + \bar{H}_{pk}^{(3)} + H_T^{(3)}, \quad (128)$$

where

$$H_S^{(3)} = \hbar\omega_1^{(3)}\sigma_{11} + \hbar\omega_2^{(3)}\sigma_{22} + \hbar\omega_3^{(3)}\sigma_{33}, \quad (129)$$

$$\bar{H}_{pk}^{(3)} = -M\bar{I}^{(3)}(t)I_{pk}(0, t), \quad (130)$$

$$H_T^{(3)} = -M\bar{I}^{(3)}(t)(I_L(0, t) + I_R(0, t)). \quad (131)$$

Here, the loop current  $\bar{I}^{(3)}(t) = U_r^{(3)\dagger}\hat{I}^{(3)}(t)U_r^{(3)}$  and its matrix elements have been listed in Appendix. C. Here,  $H_S^{(3)}$  is treated as the system Hamiltonian originating from the first three terms in Eq. (73). In Eq. (75), the eigen frequencies are respectively

$$\omega_1^{(3)} = \frac{1}{2} \left( \Delta_{31,3} - \sqrt{4\Omega_{31,1}^2 + \Delta_{31,3}^2} \right), \quad (132)$$

$$\omega_2^{(3)} = \omega_{21}, \quad (133)$$

$$\omega_3^{(3)} = \frac{1}{2} \left( \Delta_{31,3} + \sqrt{4\Omega_{31,1}^2 + \Delta_{31,3}^2} \right). \quad (134)$$

The Hamiltonian  $\bar{H}_{pk}^{(3)}$  is a small quantity compared to  $H_S^{(3)}$  and hence will be treated as the perturbation to the system Hamiltonian. Besides,  $H_T^{(3)}$  determines the dissipation of the system into the 1D open space. With fast oscillating terms neglected,  $\bar{H}_{pk}^{(3)}$  can be further reduced to

$$\bar{H}_{p5} = \hbar\varepsilon_{21,5}e^{-i\omega_5t}\sigma_{21} + \hbar\varepsilon_{32,5}e^{-i\omega_5t}\sigma_{23} + \text{h.c.} \quad (135)$$

$$\bar{H}_{p6} = \hbar\varepsilon_{21,6}e^{i\omega_6-t}\sigma_{12} + \hbar\varepsilon_{32,6}e^{i\omega_6-t}\sigma_{32} + \text{h.c.} \quad (136)$$

where  $\omega_{6-} = \omega_{d3} - \omega_6$  is the produced difference fre-

quency, and the coupling energy parameters are

$$\hbar\varepsilon_{21,5} = \frac{-M \cos \frac{\theta_3}{2} \tilde{I}_{p5}(0) I_{21}}{2}, \quad (137)$$

$$\hbar\varepsilon_{32,5} = \frac{-M \sin \frac{\theta_3}{2} \tilde{I}_{p5} I_{21}}{2}, \quad (138)$$

$$\hbar\varepsilon_{21,6} = \frac{M \sin \frac{\theta_3}{2} \tilde{I}_{p6} I_{32}}{2}, \quad (139)$$

$$\hbar\varepsilon_{32,6} = \frac{-M \cos \frac{\theta_3}{2} \tilde{I}_{p6} I_{32}}{2}. \quad (140)$$

### B. Dynamics of the system and its solutions

Using the detailed parameters of  $\bar{I}^{(3)}(t)$  in Appendix C, we can derive that the reduced density matrix  $s$  of the system is governed by the following master equation [55]

$$\frac{\partial s}{\partial t} = \frac{1}{i\hbar} [H_S^{(3)} + \bar{H}_{pk}^{(3)}, s] + \mathcal{L}[s]. \quad (141)$$

We must mention we work in the picture defined by unitary transformations  $U_d^{(1)}$  and  $U_r^{(1)}$ . The dissipation of the system is described via the Lindblad term

$$\begin{aligned} \mathcal{L}[s] = & \sum_m \left( \sum_{k \neq m} \gamma_{km}^{(3)} s_{kk} - \sum_{k \neq m} \gamma_{mk}^{(3)} s_{mm} \right) \sigma_{mm} \\ & - \sum_{m \neq n} \frac{1}{2} \Gamma_{mn}^{(2)} s_{mn} \sigma_{mn}. \end{aligned} \quad (142)$$

Here,  $s_{mn} \equiv s_{mn}(t)$  are matrix elements of the reduced density operator  $s(t)$ . The relaxation and dephasing rates can be calculated as  $\gamma_{mn}^{(3)} = \frac{M^2}{\hbar Z_T} K_{mn}^{(3)}$  and  $\Gamma_{mn}^{(3)} = \frac{M^2}{\hbar Z_T} \left( \sum_{k \neq m} K_{mk}^{(3)} + \sum_{k \neq n} K_{nk}^{(3)} + K_{\phi mn}^{(3)} \right)$  from hypotheses (1), (2), and (4) in Sec. II. The explicit expressions of  $K_{mn}^{(3)}$  and  $K_{\phi mn}^{(3)}$  given in Appendix C.

Then we seek the solutions of Eq. (86) in the form of a power series expansion in the magnitude of  $\bar{H}_{pk}^{(3)}$ , that is, a solution of the form

$$s(t) = s^{(0)}(t) + s^{(1)}(t) + \cdots + s^{(r)}(t) + \cdots, \quad (143)$$

for the reduced density matrix  $s$  of the three-level system. Here,  $s^{(0)}$  is the steady state solution when no signal field is applied to the system. However, the  $r$ th-order reduced density matrix  $s^{(r)}(t)$  is proportional to  $r$ th order of  $\bar{H}_{pk}^{(3)}$ .

In the first order approximation, we have

$$\frac{\partial s^{(0)}}{\partial t} = \frac{1}{i\hbar} [H_S^{(3)}, s^{(0)}] + \mathcal{L}[s^{(0)}], \quad (144)$$

$$\frac{\partial s^{(1)}}{\partial t} = \frac{1}{i\hbar} [H_S^{(2)}, s^{(1)}] + \frac{1}{i\hbar} [\bar{H}_{pk}^{(3)}, s^{(0)}] + \mathcal{L}[s^{(1)}]. \quad (145)$$

The solutions of Eq. (144) are

$$s_{11}^{(0)} = \frac{\lambda_{21}}{\lambda_{21}y_3^2 + \lambda_{32}y_3 + \lambda_{21}}, \quad (146)$$

$$s_{22}^{(0)} = \frac{y_3\lambda_{32}}{\lambda_{21}y_3^2 + \lambda_{32}y_3 + \lambda_{21}}, \quad (147)$$

$$s_{33}^{(0)} = \frac{y_3^2\lambda_{21}}{\lambda_{21}y_3^2 + \lambda_{32}y_3 + \lambda_{21}}, \quad (148)$$

all of which are  $\lambda_{31}$  independent. And the other terms of  $s^{(0)}$  are all zeros. Having obtained  $s^{(0)}$ , we can future solve Eq. (145). When  $\bar{H}_{pk}^{(3)}$  takes  $\bar{H}_{p5}^{(3)}$ , we have the nonzero matrix elements of  $s^{(1)}$  as follows,

$$s_{21}^{(1)} = s_{12}^{(1)*} = \frac{i\varepsilon_{21,5} e^{-i\omega_5 t} (s_{22}^{(0)} - s_{11}^{(0)})}{i(\omega_{21}^{(3)} - \omega_5) + \frac{1}{2}\Gamma_{21}^{(3)}}, \quad (149)$$

$$s_{32}^{(1)} = s_{23}^{(1)*} = \frac{i\varepsilon_{32,5}^* e^{i\omega_5 t} (s_{33}^{(0)} - s_{22}^{(0)})}{i(\omega_{32}^{(3)} + \omega_5) + \frac{1}{2}\Gamma_{32}^{(3)}}. \quad (150)$$

when  $\bar{H}_{pk}^{(3)}$  takes  $\bar{H}_{p6}^{(3)}$ , we have the nonzero matrix elements of  $s^{(1)}$  as follows,

$$s_{21}^{(1)} = s_{12}^{(1)*} = \frac{i\varepsilon_{21,6}^* e^{-i\omega_6 t} (s_{22}^{(0)} - s_{11}^{(0)})}{-i(\omega_{6-} - \omega_{21}^{(3)}) + \frac{1}{2}\Gamma_{21}^{(3)}}, \quad (151)$$

$$s_{32}^{(1)} = s_{23}^{(1)*} = \frac{i\varepsilon_{32,6} e^{i\omega_6 t} (s_{33}^{(0)} - s_{22}^{(0)})}{i(\omega_{6-} + \omega_{32}^{(3)}) + \frac{1}{2}\Gamma_{32}^{(3)}}. \quad (152)$$

### C. Scattered current

The scattered current at  $x = 0$ , similarly to driving type (1), can be represented by

$$I_{s3}(0, t) = -\frac{iM}{2Z_T} \sum_{mnk} \delta_{mnk}^{(3)} \bar{I}_{mnk}^{(3)} e^{i\nu_{mnk}^{(3)} t} s_{nm}, \quad (153)$$

with  $\delta_{mnk}^{(3)} = \omega_{mn}^{(3)} + \nu_{mnk}^{(3)}$ . Here, we have assumed that the matrix element of  $\bar{I}^{(3)}(t)$  is of the form  $\bar{I}_{mn}^{(3)}(t) = \sum_k \bar{I}_{mnk}^{(3)} e^{i\nu_{mnk}^{(3)} t}$ . We hereby also expand the scattered current as  $I_{s3} = \sum_{r=0}^{\infty} I_{s3}^{(r)}$ , where  $I_{s3}^{(r)}$  is in the  $r$ th order of  $\bar{H}_{pk}^{(3)}$ . In this present paper, we are only interested in the linear response of  $\bar{H}_{pk}^{(3)}$ , that is,

$$I_{s3}^{(1)}(0, t) = -\frac{iM}{2Z_T} \sum_{mnk} \delta_{mnk}^{(3)} \bar{I}_{mnk}^{(3)} e^{i\nu_{mnk}^{(3)} t} s_{nm}^{(1)}. \quad (154)$$

### D. Probe type (5)

When  $H_{pk}^{(3)}$  takes  $H_{p5}^{(3)}$ , using Eqs. (149)-(150), we have the linear response as

$$I_{s3}^{(1)}(0, t) = \text{Re}\{\tilde{I}_{s3}(\omega_5)e^{-i\omega_5 t}\} + \text{Re}\{\tilde{I}_{s5}(\omega_{5+})e^{-i\omega_{5+} t}\} \quad (155)$$

where  $\omega_{5+} = \omega_{d3} - \omega_{5+}$  is the produced difference frequency. The amplitudes of both frequency components are respectively  $\tilde{I}_{s3}(\omega_5)$  and  $\tilde{I}_{s5}(\omega_{5+})$ . The gain of the incident current  $I_{p5}$  is defined as  $G_5 = 1 + \tilde{I}_{s3}(\omega_5)/\tilde{I}_{p5}$ , and the explicit expression is

$$G_5 = 1 + \frac{M^2}{2\hbar Z_T} \frac{(s_{22}^{(0)} - s_{11}^{(0)}) \lambda_{21} \cos^2 \frac{\theta_3}{2}}{i(\omega_{21}^{(3)} - \omega_5) + \frac{1}{2}\Gamma_{21}^{(3)}} - \frac{M^2}{2\hbar Z_T} \frac{(s_{33}^{(0)} - s_{22}^{(0)}) \lambda_{21} \sin^2 \frac{\theta_3}{2}}{i(\omega_{32}^{(3)} + \omega_5) + \frac{1}{2}\Gamma_{32}^{(3)}} \quad (156)$$

Meanwhile, the corresponding efficiency of frequency down conversion is defined as  $\eta_5 = \tilde{I}_{s3}(\omega_{5+})/\tilde{I}_{p5}\sqrt{\omega_5/\omega_{5+}}$  since  $|\eta_5|^2$  represents the photon number of frequency  $\omega_{5+}$  produced by each photon of frequency  $\omega_5$  per unit time. The explicit expression of  $\eta_5$  is hence

$$\eta_5 = \frac{M^2 \sqrt{\lambda_{32}\lambda_{21}} \cos \frac{\theta_3}{2} \sin \frac{\theta_3}{2}}{2\hbar Z_T} \left[ \frac{(s_{22}^{(0)} - s_{11}^{(0)})}{i(\omega_{21}^{(3)} - \omega_5) + \frac{1}{2}\Gamma_{21}^{(3)}} + \frac{(s_{33}^{(0)} - s_{22}^{(0)})}{i(\omega_{32}^{(3)} + \omega_5) + \frac{1}{2}\Gamma_{32}^{(3)}} \right] \exp(-i \arg \tilde{I}_{p5}). \quad (157)$$

The two resonant points of  $G_5$  and  $\eta_5$  are respectively at  $\omega_5 = \omega_{21}^{(3)}$  and  $\omega_5 = \omega_{32}^{(3)}$ . As we have assumed a sufficiently large  $\Omega_{31,3}$ , the two points must be well separated. Therefore, we can determine from Eq. (156) that the transmitted signal with frequency  $\omega_5$  can be both attenuated and amplified depending on the sign of  $s_{22}^{(0)} - s_{11}^{(0)}$  or  $s_{33}^{(0)} - s_{22}^{(0)}$ . At both points,  $|G_5|$  reaches the maximum or minimum gain, while  $|\eta_5|$  reaches the maximum conversion efficiency. To obtain the optimal attenuation, amplification, or conversion efficiency, we can first minimize  $\Gamma_{21}^{(3)}$  and  $\Gamma_{32}^{(3)}$  whose expressions are respectively

$$\Gamma_{21}^{(3)} = \frac{M^2}{\hbar Z_T} \left( \lambda_{21} \cos^2 \frac{\theta_3}{2} + \sin^2 \frac{\theta_3}{2} \lambda_{\text{sum}} \right), \quad (158)$$

$$\Gamma_{32}^{(3)} = \frac{M^2}{\hbar Z_T} \left( \sin^2 \frac{\theta_3}{2} \lambda_{21} + \cos^2 \frac{\theta_3}{2} \lambda_{\text{sum}} \right). \quad (159)$$

Here,  $\lambda_{\text{sum}} = \lambda_{21} + \lambda_{32} + \lambda_{31}$ . The dephasing rates  $\Gamma_{21}^{(3)}$  and  $\Gamma_{32}^{(3)}$  can be further reduced to

$$\Gamma_{21}^{(3)} = \frac{M^2}{\hbar Z_T} \left[ \lambda_{21} \cos^2 \frac{\theta_3}{2} + \sin^2 \frac{\theta_3}{2} (\lambda_{21} + \lambda_{32}) \right], \quad (160)$$

$$\Gamma_{32}^{(3)} = \frac{M^2}{\hbar Z_T} \left[ (\lambda_{21} + \lambda_{32}) \cos^2 \frac{\theta_3}{2} + \sin^2 \frac{\theta_3}{2} \lambda_{21} \right], \quad (161)$$

in the limit that  $\lambda_1 \ll 1$  and  $\lambda_2 \ll 1$ . We thus assume  $\lambda_1 \ll 1$  and  $\lambda_2 \ll 1$  in the following discussions of  $\eta_5$  and  $G_5$ .

When  $\omega_5$  is near  $\omega_{21}^{(3)}$ , the amplification condition (i.e.,  $s_{22}^{(0)} - s_{11}^{(0)} > 0$ ) is

$$\lambda_3 y_3 > 1, \quad (162)$$

and the attenuation condition (i.e.,  $s_{22}^{(0)} - s_{11}^{(0)} < 0$ ) is

$$\lambda_3 y_3 < 1. \quad (163)$$

We now further seek the limitation value of  $|G_5|$  when  $\omega_5 = \omega_{21}^{(3)}$ . In this case,  $G_5$  is reduced to

$$G_5 = 1 + \frac{1}{1 + y_3 + \lambda_3 y_3} \frac{\lambda_3 y_3 - 1}{y_3^2 + \lambda_3 y_3 + 1}, \quad (164)$$

with  $y_3 = \tan^2(\theta_3/2)$ . In Eq. (164),  $y_3$  and  $\lambda_3 y_3$  will be regarded as independent parameters. In the amplification case,  $|G_5|$  can be maximized, yielding

$$G_5 = 1 + \frac{1}{(\sqrt{A_1} + \sqrt{A_2})^2} \quad (165)$$

when the condition  $\lambda_3 y_3 = \sqrt{A_1 A_2} + 1$  holds. Here, parameters  $A_1$  and  $A_2$  respectively take  $A_1 = y_3 + 2$  and  $A_2 = y_3^2 + 2$ . Furthermore, the condition  $y_3 \ll 1$  yields the optimal amplification, yielding

$$G_5 = 1 + \frac{1}{8}, \quad (166)$$

where the condition for  $\lambda_3 y_3$  becomes  $\lambda_3 y_3 = 3$ . In the resonant driving case, using Eq. (165), the optimal  $G_5$  for amplification can be reduced to

$$G_5 = 1 + \frac{1}{12}, \quad (167)$$

where the conditions become  $y_3 = 1$  and  $\lambda_3 = 4$ . In the attenuation case,  $|G_5|$  can be minimized, yielding

$$G_5 = 1 - \frac{1}{y_3^3 + y_3^2 + y_3 + 1}, \quad (168)$$

when  $\lambda_3 y_3 \ll 1$ . Furthermore, the condition  $y_3 \ll 1$  yields the optimal gain for attenuation, that is,

$$G_5 = 0. \quad (169)$$

In the resonant driving case, from Eq. (168), the optimal  $G_5$  for attenuation can be reduced to

$$G_5 = \frac{3}{4}, \quad (170)$$

where the conditions are  $y_3 = 1$  and  $\lambda_3 \ll 1$ . In Fig. 7(a),  $\eta_5$  takes Eq. (164). We have plotted  $|G_5|$  as the function of  $\lambda_3 y_3$  when  $y_3$  takes 0, 1, and 4, respectively. When  $\lambda_3 y_3$  increases from  $\lambda_3 y_3 < 1$ , to  $\lambda_3 y_3 = 1$ , and then to

$\lambda_3 y_3 > 1$ ,  $|G_5|$  sequentially exhibits attenuation ( $|G_5| < 1$ ), transparency ( $|G_5| = 1$ ), and amplification ( $|G_5| > 1$ ). Despite the regime of  $\lambda_3 y_3$ , the increase of  $y_3$  will always weaken the attenuation or amplification of the probe signal.

When  $\omega_5$  is near  $-\omega_{32}^{(3)}$ , The amplification condition (i.e.,  $s_{33}^{(0)} - s_{22}^{(0)} < 0$ ) is

$$\lambda_3 y_3^{-1} > 1, \quad (171)$$

and the attenuation condition (i.e.,  $s_{33}^{(0)} - s_{22}^{(0)} > 0$ ) is

$$\lambda_3 y_3^{-1} < 1. \quad (172)$$

We now further seek the limitation value of  $|G_5|$  when  $\omega_5 = -\omega_{32}^{(3)}$ . In this case,  $G_5$  is reduced to

$$G_5 = 1 + \frac{1}{1 + y_3^{-1} + \lambda_3 y_3^{-1}} \frac{\lambda_3 y_3^{-1} - 1}{1 + \lambda_3 y_3^{-1} + y_3^{-2}}. \quad (173)$$

The similarity can be easily seen between Eqs. (173) and (164). We thus directly have that in the amplification case, the gain  $G_5$  for amplification can be maximized as

$$G_5 = 1 + \frac{1}{(\sqrt{B_1} + \sqrt{B_2})^2} \quad (174)$$

when  $\lambda_3 y_3^{-1} = \sqrt{B_1 B_2} + 1$  with  $B_1 = y_3^{-1} + 2$ ,  $B_2 = y_3^{-2} + 2$ . Furthermore, optimal gain for amplification can be achieved as

$$G_5 = 1 \frac{1}{8}, \quad (175)$$

when  $y_3^{-1} \ll 1$  and  $\lambda_3 y_3^{-1} = 3$ . From Eq. (174), the optimal gain for amplification can be reduced to

$$G_5 = 1 \frac{1}{12}, \quad (176)$$

in the resonant driving case where the conditions are  $y_3 = 1$ , and  $\lambda_3 = 4$ . In the attenuation case, the gain for attenuation can be minimized as

$$G_5 = 1 - \frac{1}{y_3^{-3} + y_3^{-2} + y_3^{-1} + 1}, \quad (177)$$

when  $\lambda_3 y_3^{-1} \ll 1$ . Furthermore, the condition  $y_3^{-1} \ll 1$  yields the optimal gain for attenuation, that is,

$$G_5 = 0. \quad (178)$$

From Eq. (177), the optimal  $G_5$  for attenuation can be reduced to

$$G_5 = \frac{3}{4}, \quad (179)$$

in the resonant driving case where the condition are  $y_3 = 1$  and  $\lambda_3 \ll 1$ . The behaviours of  $|G_5|$  can be similarly explained through Fig. 7(a) when  $G_5$  takes Eq. (173).

We now seek the limitation of  $|\eta_5|$  when  $\omega_5 = \omega_{21}^{(3)}$ . In this case, the conversion efficiency  $\eta_5$  is reduced to

$$\eta_5 = \frac{\exp(-i \arg \tilde{I}_{p5}) \sqrt{\lambda_3 y_3}}{1 + y_3 + \lambda_3 y_3} \frac{\lambda_3 y_3 - 1}{1 + \lambda_3 y_3 + y_3^2}. \quad (180)$$

Here,  $y_3$  and  $\lambda_3 y_3$  will be continuously treated as independent. When  $y_3 \ll 1$ , the conversion efficiency  $\eta_5$  can be maximized as

$$\eta_5 = \frac{\exp(-i \arg \tilde{I}_{p5}) \sqrt{\lambda_3 y_3}}{1 + \lambda_3 y_3} \frac{\lambda_3 y_3 - 1}{1 + \lambda_3 y_3}. \quad (181)$$

Furthermore, the condition  $\lambda_3 y_3 = 3 \pm 2\sqrt{2}$  yields the optimal conversion efficiency as

$$\eta_5 = \pm \frac{1}{4} \exp(-i \arg \tilde{I}_{p5}). \quad (182)$$

In the resonant driving case,  $y_3 = 1$ , and the optimal conversion efficiency reads

$$\eta_5 = 0.19838 \exp(-i \arg \tilde{I}_{p5}). \quad (183)$$

under the condition  $\lambda_3 = (9 + \sqrt{73})/2$ . In Fig. 7(b),  $\eta_5$  takes Eq. (180). We have plotted  $|\eta_5|$  as the functions of  $\lambda_3 y_3$  when  $y_3$  takes 0, 1, and 2, respectively. When  $\lambda_3 y_3 = 1$ , we can see  $|\eta_5| = 0$ , indicating the switch off of conversion process. Besides this point, there are two peaks. When  $y_3 = 0$ , the two peaks are of the same value. When  $y_3$  takes 1 and 2, the peak at the right takes the largest value. Besides, the larger value  $y_3$  takes, the smaller  $|\eta_5|$  becomes. It is a similar case when  $\omega_{5+} = -\omega_{32}^{(3)}$ , where the conversion efficiency becomes

$$\eta_5 = \frac{(1 - \lambda_3 y_3^{-1}) \sqrt{\lambda_3 y_3^{-1}} \exp(-i \arg \tilde{I}_{p5})}{(1 + \lambda_3 y_3^{-1} + y_3^{-2}) (\lambda_3 y_3^{-1} + y_3^{-1} + 1)}. \quad (184)$$

The similarity can be easily found between Eqs. (184) and (180). Thus, it can be directly given that at  $y_3^{-1} \ll 1$  and  $\lambda_3 y_3^{-1} = 3 \pm 2\sqrt{2}$ , the optimal conversion efficiency reads

$$\eta_5 = \mp \frac{1}{4} \exp(-i \arg \tilde{I}_{p5}). \quad (185)$$

In the resonant driving case,  $y_3 = 1$ , and the optimal conversion efficiency reads

$$\eta_5 = -0.19838 \quad (186)$$

when  $\lambda_3 = (9 + \sqrt{73})/2$ . When  $\eta_5$  takes Eq. (184), the behaviours of  $|\eta_5|$  can also be explained though Fig. 7(b).

### E. Probe type (6)

When  $H_{pk}^{(2)}$  takes  $H_{p6}^{(2)}$ , using Eqs. (151)-(152), we have the linear response as

$$I_{s3}^{(1)}(0, t) = \text{Re}\{\tilde{I}_{s3}(\omega_6) e^{-i\omega_6 t}\} + \text{Re}\{\tilde{I}_{s3}(\omega_{6-}) e^{-i\omega_{6-} t}\}. \quad (187)$$



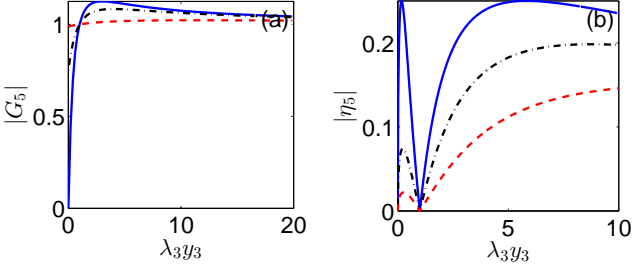


FIG. 7: (Color online) Probe type (5), driving type (3). The gain (a)  $|G_5|$  and conversion efficiency (b)  $|\eta_5|$  plotted as functions of  $\lambda_3 y_3$ . Here, we have assumed that  $\omega_5 = \omega_{21}^{(3)}$  and  $\lambda_1, \lambda_2 \ll 1$ . In (a),  $y_3 = 0$  (solid blue), 1 (dash-dotted black), and 4 (dashed red), respectively. In (b),  $y_3 = 0$  (solid blue), 1 (dash-dotted black), and 2 (dashed red), respectively.

The amplitudes of both frequency components are respectively  $\tilde{I}_{s3}(\omega_6)$  and  $\tilde{I}_{s3}(\omega_{6-})$ . The gain of the incident current  $I_{p6}$  is defined as  $G_6 = 1 + \tilde{I}_{s3}(\omega_6) / \tilde{I}_{p6}$ , and the explicit expression is

$$G_6 = 1 - \frac{M^2}{2\hbar Z_T} \frac{\lambda_{32} \sin^2 \frac{\theta_3}{2} (s_{22}^{(0)} - s_{11}^{(0)})}{i(\omega_{6-} - \omega_{21}^{(3)}) + \frac{1}{2}\Gamma_{21}^{(3)}} + \frac{M^2}{2\hbar Z_T} \frac{\lambda_{32} \cos^2 \frac{\theta_3}{2} (s_{33}^{(0)} - s_{22}^{(0)})}{i(\omega_{6-} + \omega_{32}^{(3)}) + \frac{1}{2}\Gamma_{32}^{(3)}}. \quad (188)$$

Meanwhile, the corresponding efficiency of frequency down conversion is defined as  $\eta_6 = \tilde{I}(\omega_{6-}) / \tilde{I}_{p6} \sqrt{\omega_6 / \omega_{6-}}$  since  $|\eta_6|^2$  represents the photon number of frequency  $\omega_{6-}$  produced by each photon of frequency  $\omega_6$  per unit time. The explicit expression of  $\eta_6$  is hence

$$\eta_6 = \frac{M^2 \sqrt{\lambda_{21} \lambda_{32}} \sin \frac{\theta_3}{2} \cos \frac{\theta_3}{2}}{-2\hbar Z_T} \left[ \frac{(s_{22}^{(0)} - s_{11}^{(0)})}{-i(\omega_{6-} - \omega_{21}^{(3)}) + \frac{1}{2}\Gamma_{21}^{(3)}} + \frac{(s_{33}^{(0)} - s_{22}^{(0)})}{-i(\omega_{6-} + \omega_{32}^{(3)}) + \frac{1}{2}\Gamma_{32}^{(3)}} \right] \exp(-i \arg \tilde{I}_{p6}). \quad (189)$$

The two resonant points of  $G_6$  and  $\eta_6$  are respectively at  $\omega_{6-} = \omega_{21}^{(3)}$  and  $\omega_{6-} = -\omega_{32}^{(3)}$ . As we have assumed a sufficiently large  $\Omega_{31,3}$ , the two points must be well separated. Therefore, we can determine from Eq. (56) that the transmitted signal with frequency  $\omega_6$  can be both attenuated or amplified. At both points,  $|G_6|$  reaches the maximum gain and maximum conversion efficiency, while  $|\eta_6|$  reaches the maximum conversion efficiency. We will similarly assume  $\lambda_1 \ll 1$  and  $\lambda_2 \ll 1$  as in probe type (5) in the following discussions of  $\eta_6$  and  $G_6$ .

We now further seek the limitation value of  $|G_6|$  when  $\omega_{6-} = \omega_{21}^{(3)}$ . In this case,  $G_6$  is reduced to

$$G_6 = 1 - \frac{y_3 \lambda_3}{1 + y_3 + y_3 \lambda_3} \frac{y_3 \lambda_3 - 1}{1 + y_3 \lambda_3 + y_3^2}. \quad (190)$$

In the amplification case, the gain can be maximized as

$$G_6 = 1 + \frac{1}{(\sqrt{A_1 A_4} + \sqrt{A_2 A_3})^2}, \quad (191)$$

when  $\lambda_3 y_3 = (\sqrt{A_1 A_2 / A_3 A_4} + 1)^{-1}$  with  $A_3 = y_3 + 1$ , and  $A_4 = y_3^2 + 1$ . Furthermore, the condition  $y_3 \ll 1$  yields the optimal gain for amplification, i.e.,

$$G_6 = 1 + \frac{1}{8}, \quad (192)$$

where the condition for  $\lambda_3 y_3$  becomes  $\lambda_3 y_3 = 1/3$ . From Eq. (191), the optimal gain for amplification can be reduced to

$$G_6 = 1 + \frac{1}{24}, \quad (193)$$

in the resonant case, where the conditions are  $y_3 = 1$  and  $\lambda_3 = 2/5$ . In the attenuation case, the condition  $\lambda_3 y_3 \gg 1$  yields the optimal gain for attenuation

$$G_6 = 0. \quad (194)$$

In the resonant driving case, the conditions become  $y_3 = 1$  and  $\lambda_3 \gg 1$  where the optimal gain for attenuation is still  $G_6 = 0$ . In Fig. 8,  $G_6$  takes Eq. (190). We have plotted  $|G_6|$  as the function of  $\lambda_3 y_3$  when  $y_3$  takes 0, 1, and 4, respectively. When  $\lambda_3 y_3$  changes from  $\lambda_3 y_3 < 1$ , to  $\lambda_3 y_3 = 1$ , and then to  $\lambda_3 y_3 > 1$ ,  $|G_6|$  sequentially exhibits amplification ( $|G_6| > 1$ ), transparency ( $|G_6| = 1$ ), and attenuation ( $|G_6| < 1$ ). Despite the regime of  $\lambda_3 y_3$ , the increase of  $y_3$  will always weaken the attenuation or amplification of the probe signal. It is a similar case when  $\omega_{6-} = -\omega_{32}^{(3)}$ , where the gain becomes

$$G_6 = 1 + \frac{\lambda_3 y_3^{-1}}{1 + y_3^{-1} + \lambda_3 y_3^{-1}} \frac{1 - \lambda_3 y_3^{-1}}{1 + \lambda_3 y_3^{-1} + y_3^{-2}}. \quad (195)$$

The similarity can be easily found between Eqs. (195) and (190). Thus, we directly have that the gain for amplification can be optimized as

$$G_6 = 1 + \frac{1}{(\sqrt{B_1 B_4} + \sqrt{B_2 B_3})^2}, \quad (196)$$

when  $\lambda_3 y_3^{-1} = (\sqrt{B_1 B_2 / B_3 B_4} + 1)^{-1}$  with  $B_1 = y_3^{-1} + 2$ ,  $B_2 = y_3^{-2} + 2$ ,  $B_3 = 1 + y_3^{-1}$ , and  $B_4 = 1 + y_3^{-2}$ . Furthermore, the condition  $y_3^{-1} \ll 1$  yields the optimal gain for amplification

$$G_6 = 1 + \frac{1}{8}, \quad (197)$$

where  $\lambda_3 y_3^{-1} = 1/3$ . From Eq. (196), the gain for amplification can be reduced to

$$G_6 = 1 + \frac{1}{24}, \quad (198)$$

with the condition  $y_3 = 1$  and  $\lambda_3 = 2/5$ . In the attenuation case, the condition  $\lambda_3 y_3^{-1} \gg 1$  yields the optimal gain as

$$G_6 = 0. \quad (199)$$

In the resonant case, the conditions become  $y_3 = 1$  and  $\lambda_3 \gg 1$  where the optimal gain for attenuation is still  $G_6 = 0$ . When  $G_6$  takes Eq. (195), the behaviour of  $|G_6|$  can also be investigated through Fig. 195(a).

We now seek the limitation of  $|\eta_6|$  when  $\omega_{6-} = \omega_{21}^{(3)}$ . In this case,  $\eta_6$  is reduced to

$$\eta_6 = -\frac{\exp(-i \arg \tilde{I}_{p6}) \sqrt{\lambda_3 y_3}}{1 + y_3 + \lambda_3 y_3} \frac{\lambda_3 y_3 - 1}{1 + \lambda_3 y_3 + y_3^2}. \quad (200)$$

We find Eqs. (200) and (180) are equivalent except for a global constant. We thus directly have the optimal conversion efficiency

$$\eta_6 = \mp \frac{1}{4} \exp(-i \arg \tilde{I}_{p6}). \quad (201)$$

when  $y_3 \ll 1$  and  $\lambda_3 y_3 = 3 \pm 2\sqrt{2}$ . In the resonant driving case,  $y_3 = 1$ , and the optimal conversion efficiency becomes

$$\eta_6 = -0.19838 \exp(-i \arg \tilde{I}_{p6}), \quad (202)$$

in the condition that  $\lambda_3 = (9 + \sqrt{73})/2$ . It is a similar case when  $\omega_{6-} = -\omega_{32}^{(3)}$ , where the conversion efficiency becomes

$$\eta_6 = -\frac{\exp(-i \arg \tilde{I}_{p6}) \sqrt{\lambda_3 y_3^{-1}}}{1 + y_3^{-1} + \lambda_3 y_3^{-1}} \frac{1 - \lambda_3 y_3^{-1}}{1 + \lambda_3 y_3^{-1} + y_3^{-2}}. \quad (203)$$

With the condition  $y_3^{-1} \ll 1$  and  $\lambda_3 y_3^{-1} = 3 \pm 2\sqrt{2}$ , the optimal conversion efficiency reaches

$$\eta_6 = \pm \frac{1}{4} \exp(-i \arg \tilde{I}_{p6}). \quad (204)$$

In the resonant driving case,  $y_3 = 1$ , and we can achieve the optimal conversion efficiency as

$$\eta_6 = 0.19838 \exp(-i \arg \tilde{I}_{p6}), \quad (205)$$

when  $\lambda_3 = (9 + \sqrt{73})/2$ . For completeness, we also plot Fig. 8(b). Both Eqs. (200) and (203) can be described by Fig. 8(b).

## VI. CONCLUSIONS AND DISCUSSIONS

In summary, using a three-level three-junction flux qubit circuit as an example, we study how the frequency

conversion and signal amplification (or attenuation) can be realized when the inversion symmetry of the potential

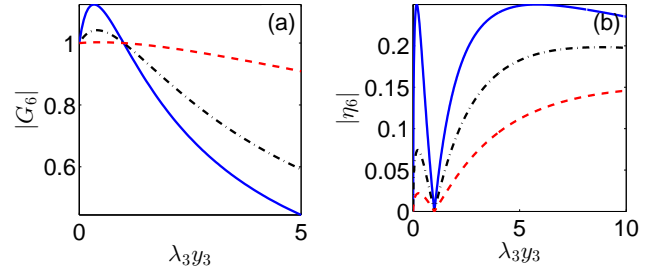


FIG. 8: (Color online) Probe type (6), driving type (3). The gain (a)  $|G_6|$  and conversion efficiency (b)  $|\eta_6|$  plotted as functions of  $\lambda_3 y_3$ . Here, we have assumed that  $\omega_{6-} = \omega_{21}^{(3)}$  and  $\lambda_1, \lambda_2 \ll 1$ . In (a),  $y_3 = 0$  (solid blue), 1 (dash-dotted black), and 4 (dashed red), respectively. In (b),  $y_3 = 0$  (solid blue), 1 (dash-dotted black), and 2 (dashed red), respectively.

energy is broken. We mention that the microwave amplification has recently been experimentally realized [34, 58] in a three-level system constructed by four-junction flux qubit circuits. However, our study provides a full picture for understanding the microwave frequency conversion and amplification (or attenuation) in the case of all possible driving and probing. As a summary, we list in Table. II the maximum (or minimum) gains and maximum conversion efficiencies at different driving and probe types. The conditions for achieving these values are also appended in this table.

Based on different configurations of the applied driving and probing fields, we classify our study into three types. We find that a single three-level superconducting flux qubit circuit is enough to complete the microwave frequency conversion, amplification (or attenuation) of weak signal fields. In particular, we find, (i) in the driving types (1) and (2), the three-level system can convert the driving and signal fields into the ones with new frequencies, which we call down conversion or up conversion, respectively. Due to the energy loss in the reflection and conversion, the incident signal field suffers the attenuation after transmitted in these two driving types; (ii) however, both amplification and attenuation can occur in the driving type (3), whether the amplification or the attenuation depends on the parameter condition; (iii) given a definite flux bias, when the driving and signal detunings are adjusted properly, the maximum conversion efficiencies and gains nearly do not depend on the driving strength.

TABLE II: Maximum or minimum gains and maximum conversion efficiencies with the corresponding conditions for achieving them. In  $|G_k|$  column,  $|G_k| < 1$  means the attenuation is optimized while  $|G_k| > 1$  means the amplification is optimized. Here,  $l$  denotes the driving type and  $k$  denotes the probe type. Additionally,  $C_d$  represents the condition relating to the driving type and  $C_p$  represents the condition relating to the probe type. In the detuned (resonant) driving case, the maximum or minimum  $|G_k|$  is achieved at the condition  $C_d \wedge C_p \wedge C_{\text{Detuned (Resonant)}}^G$  while the maximum  $|\eta_k|$  is achieved at the condition  $C_d \wedge C_p \wedge C_{\text{Detuned (Resonant)}}^\eta$ . The symbol  $A_{14} = \sqrt{A_1 A_2 / A_3 A_4}$  and  $B_{14} = \sqrt{B_1 B_2 / B_3 B_4}$ .

$l$	$C_d$	$k$	$C_p$	Detuned driving		Resonant driving		Detuned driving		Resonant driving	
				$C_{\text{Detuned}}^G$	$ G_k $	$C_{\text{Resonant}}^G$	$ G_k $	$C_{\text{Detuned}}^\eta$	$ \eta_k $	$C_{\text{Resonant}}^\eta$	$ \eta_k $
1	$\lambda_2 \gg 1$ $\lambda_3 \gg 1$	1	$\omega_1 = \omega_{31}^{(1)}$	$\lambda_1 \gg 1$ $y_1 \ll 1$	0	$\lambda_1 \gg 1$ $y_1 = 1$	$\frac{3}{4}$	$\lambda_1 = 1$ $y_1 = 0.36349$	0.19529	$\lambda_1 = 1$ $y_1 = 1$	$\frac{1}{8}$
1	$\lambda_2 \gg 1$ $\lambda_3 \gg 1$	1	$\omega_1 = \omega_{32}^{(1)}$	$\lambda_1 \gg 1$ $y_1^{-1} \ll 1$	0	$\lambda_1 \gg 1$ $y_1 = 1$	$\frac{3}{4}$	$\lambda_1 = 1$ $y_1^{-1} = 0.36349$	0.19529	$\lambda_1 = 1$ $y_1 = 1$	$\frac{1}{8}$
1	$\lambda_2 \gg 1$ $\lambda_3 \gg 1$	2	$\omega_{2+} = \omega_{31}^{(1)}$	$\lambda_1 \ll 1$ $y_1 = 0.6573$	0.72305	$\lambda_1 \ll 1$ $y_1 = 1$	$\frac{3}{4}$	$\lambda_1 = 1$ $y_1 = 0.36349$	0.19529	$\lambda_1 = 1$ $y_1 = 1$	$\frac{1}{8}$
1	$\lambda_2 \gg 1$ $\lambda_3 \gg 1$	2	$\omega_{2+} = \omega_{32}^{(1)}$	$\lambda_1 \ll 1$ $y_1^{-1} = 0.6573$	0.72305	$\lambda_1 \ll 1$ $y_1 = 1$	$\frac{3}{4}$	$\lambda_1 = 1$ $y_1^{-1} = 0.36349$	0.19529	$\lambda_1 = 1$ $y_1 = 1$	$\frac{1}{8}$
2	$\lambda_1 \gg 1$ $\lambda_3 \ll 1$	3	$\omega_{3-} = \omega_{21}^{(2)}$	$\lambda_2 y_2 \gg 1$	0	$\lambda_2 \gg 1$ $y_2 = 1$	0	$\lambda_2 y_2 = 1$	$\frac{1}{2}$	$\lambda_2 = 1$ $y_2 = 1$	$\frac{1}{2}$
2	$\lambda_1 \gg 1$ $\lambda_3 \ll 1$	3	$\omega_{3-} = \omega_{31}^{(2)}$	$\lambda_2 y_2^{-1} \gg 1$	0	$\lambda_2 \gg 1$ $y_2 = 1$	0	$\lambda_2 y_2^{-1} = 1$	$\frac{1}{2}$	$\lambda_2 = 1$ $y_2 = 1$	$\frac{1}{2}$
2	$\lambda_1 \gg 1$ $\lambda_3 \ll 1$	4	$\omega_4 = \omega_{21}^{(2)}$	$\lambda_2 y_2 \ll 1$	0	$\lambda_2 \ll 1$ $y_2 = 1$	0	$\lambda_2 y_2 = 1$	$\frac{1}{2}$	$\lambda_2 = 1$ $y_2 = 1$	$\frac{1}{2}$
2	$\lambda_1 \gg 1$ $\lambda_3 \ll 1$	4	$\omega_4 = \omega_{31}^{(2)}$	$\lambda_2 y_2^{-1} \ll 1$	0	$\lambda_2 \ll 1$ $y_2 = 1$	0	$\lambda_2 y_2^{-1} = 1$	$\frac{1}{2}$	$\lambda_2 = 1$ $y_2 = 1$	$\frac{1}{2}$
3	$\lambda_1 \ll 1$ $\lambda_2 \ll 1$	5	$\omega_5 = \omega_{21}^{(3)}$	$\lambda_3 y_3 = 3$ $y_3 \ll 1$	$1\frac{1}{8}$	$\lambda_3 = 4$ $y_3 = 1$	$1\frac{1}{12}$	$\lambda_3 y_3 = 3 \pm 2\sqrt{2}$ $y_3 \ll 1$	$\frac{1}{4}$	$\lambda_3 = (9 + \sqrt{73})/2$ $y_3 = 1$	0.19838
3	$\lambda_1 \ll 1$ $\lambda_2 \ll 1$	5	$\omega_5 = \omega_{21}^{(3)}$	$y_3 \lambda_3 \ll 1$ $y_3 \ll 1$	0	$\lambda_3 \ll 1$ $y_3 = 1$	$\frac{3}{4}$	-	-	-	-
3	$\lambda_1 \ll 1$ $\lambda_2 \ll 1$	5	$\omega_5 = -\omega_{32}^{(3)}$	$\lambda_3 y_3^{-1} = 3$ $y_3^{-1} \ll 1$	$1\frac{1}{8}$	$\lambda_3 = 4$ $y_3 = 1$	$1\frac{1}{12}$	$\lambda_3 y_3^{-1} = 3 \pm 2\sqrt{2}$ $y_3^{-1} \ll 1$	$\frac{1}{4}$	$\lambda_3 = (9 + \sqrt{73})/2$ $y_3 = 1$	0.19838
3	$\lambda_1 \ll 1$ $\lambda_2 \ll 1$	5	$\omega_5 = -\omega_{32}^{(3)}$	$\lambda_3 y_3^{-1} \ll 1$ $y_3^{-1} \ll 1$	0	$\lambda_3 \ll 1$ $y_3 \ll 1$	$\frac{3}{4}$	-	-	-	-
3	$\lambda_1 \ll 1$ $\lambda_2 \ll 1$	6	$\omega_{6-} = \omega_{21}^{(3)}$	$\lambda_3 y_3 = 1/3$ $y_3 \ll 1$	$1\frac{1}{8}$	$\lambda_3 = \frac{2}{5}$ $y_3 = 1$	$1\frac{1}{24}$	$\lambda_3 y_3 = 3 \pm 2\sqrt{2}$ $y_3 \ll 1$	$\frac{1}{4}$	$\lambda_3 = (9 + \sqrt{73})/2$ $y_3 = 1$	0.19838
3	$\lambda_1 \ll 1$ $\lambda_2 \ll 1$	6	$\omega_{6-} = \omega_{21}^{(3)}$	$\lambda_3 y_3 \gg 1$	0	$\lambda_3 \gg 1$ $y_3 = 1$	0				
3	$\lambda_1 \ll 1$ $\lambda_2 \ll 1$	6	$\omega_{6-} = -\omega_{32}^{(3)}$	$\lambda_3 y_3^{-1} = 1/3$ $y_3^{-1} \ll 1$	$1\frac{1}{8}$	$\lambda_3 = \frac{2}{5}$ $y_3 = 1$	$1\frac{1}{24}$	$\lambda_3 y_3^{-1} = 3 \pm 2\sqrt{2}$ $y_3^{-1} \ll 1$	$\frac{1}{4}$	$\lambda_3 = (9 + \sqrt{73})/2$ $y_3 = 1$	0.19838
3	$\lambda_1 \ll 1$ $\lambda_2 \ll 1$	6	$\omega_{6-} = -\omega_{32}^{(3)}$	$\lambda_3 y_3^{-1} \gg 1$	0	$\lambda_3 \gg 1$ $y_3 = 1$	0				

Although our study focuses on a three-level superconducting flux qubit circuit, the method used here can be easily applied to a superconducting phase [45–47] and Xmon [50] qubit circuits or other quantum circuits in which the inversion symmetry of their potential energy is broken. In contrast to large anharmonicity of the flux qubit circuits, the superconducting phase and Xmon qubit circuits have small anharmonicity. Therefore the information leakage should be more carefully studied when these processes are demonstrated. We note that the transmon qubit circuits [60, 61] have well defined symmetry when the effective offset charge is at the optimal point, thus the transmon qubit circuit for its three lowest energy levels has ladder-type transitions, and the three-wave mixing cannot be realized. However, when the effective offset charge is not at the optimal point, the

three-wave mixing can also occur in such system.

It is well known that single superconducting artificial atom can be strongly coupled to different quantized microwave fields through the circuit QED technique. For example, correlated emission lasing has been demonstrated using a single three-level flux qubit circuit which is coupled to two quantized microwave modes in a transmission line resonator, and a classical field is coherently converted into other two different mode fields of microwave fields. Thus, the semiclassical treatment here for microwave field can be easily modified to the quantum case. In this case, our model can be used to study controllable generation of single and entangled microwave photon states using a single artificial atom. This will be very important for quantum information processing on superconducting quantum chip.

### Acknowledgments

YXL is supported by the National Basic Research Program of China Grant No. 2014CB921401, the NSFC Grants No. 61025022, and No. 91321208. Peng was supported by ImPACT Program of Council for Science, Technology and Innovation (Cabinet Office, Government of Japan).

### Appendix A: Parameters for driving type (1)

#### 1. Expressions of $\bar{I}_{mn}^{(1)}(t)$

$$\begin{aligned}\bar{I}_{11}^{(1)}(t) &= I_{11} \cos^2 \frac{\theta_1}{2} + I_{22} \sin^2 \frac{\theta_1}{2} \\ &\quad - I_{12} \cos \frac{\theta_1}{2} \sin \frac{\theta_1}{2} \exp(-i\omega_{d1}t) \\ &\quad - I_{21} \cos \frac{\theta_1}{2} \sin \frac{\theta_1}{2} \exp(i\omega_{d1}t),\end{aligned}\quad (\text{A1})$$

$$\begin{aligned}\bar{I}_{22}^{(1)}(t) &= I_{11} \sin^2 \frac{\theta_1}{2} + I_{22} \cos^2 \frac{\theta_1}{2} \\ &\quad + I_{12} \cos \frac{\theta_1}{2} \sin \frac{\theta_1}{2} \exp(-i\omega_{d1}t)\end{aligned}\quad (\text{A2})$$

$$+ I_{21} \cos \frac{\theta_1}{2} \sin \frac{\theta_1}{2} \exp(i\omega_{d1}t), \quad (\text{A3})$$

$$\bar{I}_{33}^{(1)}(t) = I_{33}, \quad (\text{A4})$$

$$\begin{aligned}\bar{I}_{21}^{(1)}(t) &= \bar{I}_{12}^{(1)*}(t) = (I_{11} - I_{22}) \cos \frac{\theta_1}{2} \sin \frac{\theta_1}{2} \\ &\quad - I_{12} \sin^2 \frac{\theta_1}{2} \exp(-i\omega_{d1}t) \\ &\quad + I_{21} \cos^2 \frac{\theta_1}{2} \exp(i\omega_{d1}t),\end{aligned}\quad (\text{A5})$$

$$\begin{aligned}\bar{I}_{31}^{(1)}(t) &= \bar{I}_{13}^{(1)*}(t) = I_{31} \cos \frac{\theta_1}{2} \\ &\quad + I_{32} \sin \frac{\theta_1}{2} \exp(-i\omega_{d1}t),\end{aligned}\quad (\text{A6})$$

$$\begin{aligned}\bar{I}_{32}^{(1)}(t) &= \bar{I}_{23}^{(1)*}(t) = I_{31} \sin \frac{\theta_1}{2} \\ &\quad + I_{32} \cos \frac{\theta_1}{2} \exp(-i\omega_{d1}t).\end{aligned}\quad (\text{A7})$$

#### 2. Expressions of $K_{mk}^{(1)}$ and $K_{\phi mk}^{(1)}$

$$K_{\phi 21}^{(1)} = 4 \cos^2 \frac{\theta_1}{2} \sin^2 \frac{\theta_1}{2} \lambda_{21}, \quad (\text{A8})$$

$$K_{\phi 31}^{(1)} = \cos^2 \frac{\theta_1}{2} \sin^2 \frac{\theta_1}{2} \lambda_{21}, \quad (\text{A9})$$

$$K_{\phi 32}^{(1)} = \cos^2 \frac{\theta_1}{2} \sin^2 \frac{\theta_1}{2} \lambda_{21}, \quad (\text{A10})$$

$$K_{21}^{(1)} = \cos^4 \frac{\theta_1}{2} \lambda_{21}, \quad (\text{A11})$$

$$K_{12}^{(1)} = \sin^4 \frac{\theta_1}{2} \lambda_{21}, \quad (\text{A12})$$

$$K_{32}^{(1)} = \sin^2 \frac{\theta_1}{2} \lambda_{31} + \cos^2 \frac{\theta_1}{2} \lambda_{32}, \quad (\text{A13})$$

$$K_{31}^{(1)} = \cos^2 \frac{\theta_1}{2} \lambda_{31} + \sin^2 \frac{\theta_1}{2} \lambda_{32}, \quad (\text{A14})$$

$$K_{23}^{(1)} = K_{13} = 0. \quad (\text{A15})$$

### Appendix B: Parameters for driving type (2)

#### 1. Expressions of $\bar{I}_{mn}^{(2)}(t)$

$$\bar{I}_{11}^{(2)}(t) = I_{11}, \quad (\text{B1})$$

$$\begin{aligned}\bar{I}_{22}^{(2)}(t) &= I_{22} \cos^2 \frac{\theta_2}{2} + I_{33} \sin^2 \frac{\theta_2}{2} \\ &\quad - I_{23} \cos \frac{\theta_2}{2} \sin \frac{\theta_2}{2} \exp(-i\omega_{d2}t) \\ &\quad - I_{32} \cos \frac{\theta_2}{2} \sin \frac{\theta_2}{2} \exp(i\omega_{d2}t),\end{aligned}\quad (\text{B2})$$

$$\begin{aligned}\bar{I}_{33}^{(2)}(t) &= I_{22} \sin^2 \frac{\theta_2}{2} + I_{33} \cos^2 \frac{\theta_2}{2} \\ &\quad + I_{23} \cos \frac{\theta_2}{2} \sin \frac{\theta_2}{2} \exp(-i\omega_{d2}t) \\ &\quad + I_{32} \cos \frac{\theta_2}{2} \sin \frac{\theta_2}{2} \exp(i\omega_{d2}t),\end{aligned}\quad (\text{B3})$$

$$\begin{aligned}\bar{I}_{21}^{(2)}(t) &= \bar{I}_{12}^{(2)*}(t) = I_{21} \cos \frac{\theta_2}{2} \\ &\quad - I_{31} \sin \frac{\theta_2}{2} \exp(i\omega_{d2}t),\end{aligned}\quad (\text{B4})$$

$$\begin{aligned}\bar{I}_{31}^{(2)}(t) &= \bar{I}_{13}^{(2)*}(t) = I_{21} \sin \frac{\theta_2}{2} \\ &\quad + I_{31} \cos \frac{\theta_2}{2} \exp(i\omega_{d2}t),\end{aligned}\quad (\text{B5})$$

$$\begin{aligned}\bar{I}_{32}^{(2)}(t) &= \bar{I}_{23}^{(2)*}(t) = (I_{22} - I_{33}) \cos \frac{\theta_2}{2} \sin \frac{\theta_2}{2} \\ &\quad - I_{23} \sin^2 \frac{\theta_2}{2} \exp(-i\omega_{d2}t) \\ &\quad + I_{32} \cos^2 \frac{\theta_2}{2} \exp(i\omega_{d2}t).\end{aligned}\quad (\text{B6})$$

## 2. Expressions of $K_{mk}^{(2)}$ and $K_{\phi mk}^{(2)}$

$$K_{\phi 21}^{(2)} = \cos^2 \frac{\theta_2}{2} \sin^2 \frac{\theta_2}{2} \lambda_{32}, \quad (\text{B7})$$

$$K_{\phi 31}^{(2)} = \cos^2 \frac{\theta_2}{2} \sin^2 \frac{\theta_2}{2} \lambda_{32}, \quad (\text{B8})$$

$$K_{\phi 32}^{(2)} = 4 \cos^2 \frac{\theta_2}{2} \sin^2 \frac{\theta_2}{2} \lambda_{32}, \quad (\text{B9})$$

$$K_{21}^{(2)} = \lambda_{21} \cos^2 \frac{\theta_2}{2} + \lambda_{31} \sin^2 \frac{\theta_2}{2}, \quad (\text{B10})$$

$$K_{32}^{(2)} = \lambda_{32} \cos^4 \frac{\theta_2}{2}, \quad (\text{B11})$$

$$K_{31}^{(2)} = \lambda_{21} \sin^2 \frac{\theta_2}{2} + \lambda_{31} \cos^2 \frac{\theta_2}{2}, \quad (\text{B12})$$

$$K_{23}^{(2)} = \lambda_{32} \sin^4 \frac{\theta_2}{2}, \quad (\text{B13})$$

$$K_{13}^{(2)} = K_{12}^{(2)} = 0. \quad (\text{B14})$$

## Appendix C: Parameters for driving type (3)

### 1. Expressions of $\bar{I}_{mn}^{(3)}(t)$

$$\begin{aligned} \bar{I}_{11}^{(3)}(t) &= I_{11} \cos^2 \frac{\theta_3}{2} + I_{33} \sin^2 \frac{\theta_3}{2} \\ &\quad - I_{13} \cos \frac{\theta_3}{2} \sin \frac{\theta_3}{2} \exp(-i\omega_{d3}t) \\ &\quad - I_{31} \cos \frac{\theta_3}{2} \sin \frac{\theta_3}{2} \exp(i\omega_{d3}t) \end{aligned} \quad (\text{C1})$$

$$\bar{I}_{22}^{(3)}(t) = I_{22} \quad (\text{C2})$$

$$\begin{aligned} \bar{I}_{33}^{(3)}(t) &= I_{11} \sin^2 \frac{\theta_3}{2} + I_{33} \cos^2 \frac{\theta_3}{2} \\ &\quad + I_{13} \cos \frac{\theta_3}{2} \sin \frac{\theta_3}{2} \exp(-i\omega_{d3}t) \\ &\quad + I_{31} \cos \frac{\theta_3}{2} \sin \frac{\theta_3}{2} \exp(i\omega_{d3}t) \end{aligned} \quad (\text{C3})$$

$$\begin{aligned} \bar{I}_{21}^{(3)}(t) &= \bar{I}_{12}^{(3)*}(t) = I_{21} \cos \frac{\theta_3}{2} \\ &\quad - I_{23} \sin \frac{\theta_3}{2} \exp(-i\omega_{d3}t) \end{aligned} \quad (\text{C4})$$

$$\begin{aligned} \bar{I}_{31}^{(3)}(t) &= \bar{I}_{13}^{(3)*}(t) = (I_{11} - I_{33}) \cos \frac{\theta_3}{2} \sin \frac{\theta_3}{2} \\ &\quad - I_{13} \sin^2 \frac{\theta_3}{2} \exp(-i\omega_{d3}t) \\ &\quad + I_{31} \cos^2 \frac{\theta_3}{2} \exp(i\omega_{d3}t) \end{aligned} \quad (\text{C5})$$

$$\begin{aligned} \bar{I}_{32}^{(3)}(t) &= \bar{I}_{23}^{(3)*}(t) = I_{12} \sin \frac{\theta_3}{2} \\ &\quad + I_{32} \cos \frac{\theta_3}{2} \exp(i\omega_{d3}t) \end{aligned} \quad (\text{C6})$$

### 2. Expressions of $K_{mk}^{(3)}$ and $K_{\phi mk}^{(3)}$

$$K_{\phi 21}^{(3)} = \cos^2 \frac{\theta_3}{2} \sin^2 \frac{\theta_3}{2} \lambda_{31}, \quad (\text{C7})$$

$$K_{\phi 31}^{(3)} = 4 \cos^2 \frac{\theta_3}{2} \sin^2 \frac{\theta_3}{2} \lambda_{31}, \quad (\text{C8})$$

$$K_{\phi 32}^{(3)} = \cos^2 \frac{\theta_3}{2} \sin^2 \frac{\theta_3}{2} \lambda_{31}, \quad (\text{C9})$$

$$K_{21}^{(3)} = \cos^2 \frac{\theta_3}{2} \lambda_{21}, \quad (\text{C10})$$

$$K_{12}^{(3)} = \sin^2 \frac{\theta_3}{2} \lambda_{32} \quad (\text{C11})$$

$$K_{32}^{(3)} = \cos^2 \frac{\theta_3}{2} \lambda_{32}, \quad (\text{C12})$$

$$K_{23}^{(3)} = \sin^2 \frac{\theta_3}{2} \lambda_{21} \quad (\text{C13})$$

$$K_{31}^{(3)} = \cos^4 \frac{\theta_3}{2} \lambda_{31}, \quad (\text{C14})$$

$$K_{13}^{(3)} = \sin^4 \frac{\theta_3}{2} \lambda_{31} \quad (\text{C15})$$

- 
- [1] R. W. Boyd, *Nonlinear Optics* (Academic Press, New York, 2010).
- [2] R. L. Abrams, A. Yariv, and P. A. Yeh, IEEE J. Quantum Electron. **QE-13**, 79 (1977); R. L. Abrams, C. K. Asawa, T. K. Plant, and A. E. Popa, *ibid.* **QE-13**, 82 (1977).
- [3] W. Gordy and R. L. Cook, *Microwave Molecular Spectra* (Wiley, New York, 1984).
- [4] D. Patterson and J. M. Doyle, Phys. Rev. Lett. **111**, 023008 (2013).
- [5] Z. Y. Xue, L. N. Yang, and J. Zhou, Appl. Phys. Lett. **107**, 023102 (2015).
- [6] Y. X. Liu, H. C. Sun, Z. H. Peng, A. Miranowicz, J. S. Tsai, and F. Nori, Sci. Rep. **4**, 7289 (2014).
- [7] Y. Makhlin, G. Schön, and A. Shnirman, Rev. Mod. Phys. **73**, 357 (2001).
- [8] G. Wendin and V. S. Shumeiko, cond-mat/0508729.
- [9] J. Clarke and F. K. Wilhelm, Nature (London) **453**, 1031 (2008).
- [10] Z. L. Xiang, S. Ashhab, J. Q. You, and F. Nori, Rev. Mod. Phys. **85**, 623 (2013).
- [11] J. Q. You and F. Nori, Phys. Today **58**(11), 42 (2005).
- [12] J. Q. You and F. Nori, Nature (London) **474**, 589 (2011).
- [13] R. J. Schoelkopf and S. M. Girvin, Nature (London) **451**, 664 (2008).
- [14] Y. X. Liu, C. P. Sun, and F. Nori, Phys. Rev. A **74**, 052321 (2006).
- [15] C. Cohen-Tannoudji, J. Dupont-Roc, and G. Grynberg, *Atom-Photon Interactions: Basic Process and Applications* (Wiley-VCH, Weinheim, 1998).
- [16] C. M. Wilson, T. Duty, F. Persson, M. Sandberg, G. Johansson, and P. Delsing, Phys. Rev. Lett. **98**, 257003 (2007).
- [17] C. M. Wilson, G. Johansson, T. Duty, F. Persson, M. Sandberg, and P. Delsing, Phys. Rev. B **81**, 024520 (2010).
- [18] M. Baur, S. Filipp, R. Bianchetti, J. M. Fink, M. Göppl, L. Steffen, P. J. Leek, A. Blais, and A. Wallraff, Phys. Rev. Lett. **102**, 243602 (2009).
- [19] M. A. Sillanpää, J. Li, K. Cicak, F. Altomare, J. I. Park, R. W. Simmonds, G. S. Paraoanu, and P. J. Hakonen, Phys. Rev. Lett. **103**, 193601 (2009).
- [20] J. Li, G. S. Paraoanu, K. Cicak, F. Altomare, J. I. Park, R. W. Simmonds, M. A. Sillanpää, and P. J. Hakonen, Phys. Rev. B **84**, 104527 (2011); Sci. Rep. **2**, 645 (2012).
- [21] A. A. Abdumalikov, Jr., O. Astafiev, A. M. Zagoskin, Yu. A. Pashkin, Y. Nakamura, and J. S. Tsai, Phys. Rev. Lett. **104**, 193601 (2010).
- [22] P. M. Anisimov, J. P. Dowling, and B. C. Sanders, Phys. Rev. Lett. **107**, 163604 (2011).
- [23] I.-C. Hoi, C. M. Wilson, G. Johansson, J. Lindkvist, B. Peropadre, T. Palomaki, and P. Delsing, New J. Phys. **15**, 025011 (2013).
- [24] S. Novikov, J. E. Robinson, Z. K. Keane, B. Suri, F. C. Wellstood, and B. S. Palmer, Phys. Rev. B **88**, 060503(R) (2013).
- [25] W. R. Kelly, Z. Dutton, J. Schlafer, B. Mookerji, and T. A. Ohki, J. S. Kline, and D. P. Pappas, Phys. Rev. Lett. **104**, 163601 (2010).
- [26] C. P. Yang, S.-I. Chu, and S. Han, Phys. Rev. Lett. **92**, 117902(2004).
- [27] K. V. R. M. Murali, Z. Dutton, W. D. Oliver, D. S. Crankshaw, and T. P. Orlando, Phys. Rev. Lett. **93**, 087003 (2004).
- [28] Z. Dutton, K. V. R. M. Murali, W. D. Oliver, and T. P. Orlando, Phys. Rev. B **73**, 104516 (2006).
- [29] H. Ian, Y. X. Liu, and F. Nori, Phys. Rev. A **81**, 063823 (2010).
- [30] Hui-Chen Sun, Yu-xi Liu, J. Q. You, E. Il'ichev, and F. Nori, Phys. Rev. A **89**, 063822 (2014).
- [31] Y. X. Liu, J. Q. You, L. F. Wei, C. P. Sun, and F. Nori, Phys. Rev. Lett. **95**, 087001 (2005).
- [32] T. P. Orlando, J. E. Mooij, Lin Tian, Caspar H. van der Wal, L. S. Levitov, Seth Lloyd, and J. J. Mazo, Phys. Rev. B **60**, 15398 (1999).
- [33] F. Deppe, M. Mariani, E. P. Menzel, A. Marx, S. Saito, K. Kakuyanagi, H. Tanaka, T. Meno, K. Semba, H. Takayanagi, E. Solano, and R. Gross, Nature Phys. **4**, 686 (2008).
- [34] O. V. Astafiev, A. A. Abdumalikov, Jr., A. M. Zagoskin, Yu. A. Pashkin, Y. Nakamura, and J. S. Tsai, Phys. Rev. Lett. **104**, 183603 (2010).
- [35] G. Oelsner, P. Macha, O. V. Astafiev, E. Il'ichev, M. Grajcar, U. Hübner, B. I. Ivanov, P. Neillinger, and H. G. Meyer, Phys. Rev. Lett. **110**, 053602 (2013).
- [36] S. N. Shevchenko, G. Oelsner, Ya. S. Greenberg, P. Macha, D. S. Karpov, M. Grajcar, U. Hübner, A. N. Omelyanchouk, and E. Il'ichev, Phys. Rev. B **89**, 184504 (2014).
- [37] F. Lecocq, I. M. Pop, I. Matei, E. Dumur, A. K. Feofanov, C. Naud, W. Guichard, and O. Buisson, Phys. Rev. Lett. **108**, 107001 (2012).
- [38] K. Moon and S. M. Girvin, Phys. Rev. Lett. **95**, 140504 (2005).
- [39] N. Roch, E. Flurin, F. Nguyen, P. Morfin, P. Campagne-Ibarcq, M. H. Devoret, and B. Huard, Phys. Rev. Lett. **108**, 147701 (2012).
- [40] F. Schackert, A. Roy, M. Hatridge, M. H. Devoret, and A. D. Stone, Phys. Rev. Lett. **111**, 073903 (2013).
- [41] M. A. Castellanos-Beltran, K. D. Irwin, G. C. Hilton, L. R. Vale, and K. W. Lehnert, Nat. Phys. **4**, 928 (2008).
- [42] T. Yamamoto, K. Inomata, M. Watanabe, K. Matsuba, T. Miyazaki, W. D. Oliver, Y. Nakamura, and J. S. Tsai, Appl. Phys. Lett. **93**, 042510 (2008).
- [43] N. Bergeal, F. Schackert, M. Metcalfe, R. Vijay, V. E. Manucharyan, L. Frunzio, D. E. Prober, R. J. Schoelkopf, S. M. Girvin, and M. H. Devoret, Nature **465**, 64 (2010).
- [44] N. Bergeal, R. Vijay, V. E. Manucharyan, I. Siddiqi, R. J. Schoelkopf, S. M. Girvin, and M. H. Devoret, Nat. Phys. **6**, 296 (2010).
- [45] J. M. Martinis, S. Nam, J. Aumentado, and C. Urbina, Phys. Rev. Lett. **89**, 117901 (2002).
- [46] J. Li, G. S. Paraoanu, K. Cicak, F. Altomare, J. I. Park, R. W. Simmonds, M. A. Sillanpää, and P. J. Hakonen, Phys. Rev. B **84**, 104527 (2011).
- [47] J. Li, G. S. Paraoanu, K. Cicak, F. Altomare, J. I. Park, R. W. Simmonds, M. A. Sillanpää, and P. J. Hakonen, (Nature) Sci. Rep. **2**, 645 (2012).
- [48] V. E. Manucharyan, J. Koch, L. I. Glazman, and M. H. Devoret, Science **326**, 113 (2009).
- [49] I. M. Pop, K. Geerlings, G. Catelani, R. J. Schoelkopf, L. I. Glazman, and M. H. Devoret, Nature **508**, 369 (2014).

- [50] R. Barends, J. Kelly, A. Megrant, D. Sank, E. Jeffrey, Y. Chen, Y. Yin, B. Chiaro, J. Mutus, C. Neill, P. O'Malley, P. Roushan, J. Wenner, T. C. White, A. N. Cleland, and John M. Martinis Phys. Rev. Lett. **111**, 080502 (2013).
- [51] M. H. Devoret, in *Quantum Fluctuations (Les Houches Session LXIII)*, edited by S. Reynaud, E. Giacobino, and J. Zinn-Justin (Elsevier, 1997), pp. 351.
- [52] B. Yurke and J. S. Denker, Phys. Rev. A **29**, 1419 (1984).
- [53] C. Gardiner and M. Collett, Phys. Rev. A **31**, 3761 (1985).
- [54] C. Gardiner and P. Zoller, *Quantum Noise: a Handbook of Markovian and Non-Markovian Quantum Stochastic Methods with Applications to Quantum Optics* (Springer, Berlin, 2000), Vol. **56**.
- [55] D. F. Walls and G. G. J. Milburn, *Quantum Optics* (Springer, Berlin, 2008).
- [56] C. Gardiner, A. Parkins, and P. Zoller, Phys. Rev. A **46**, 4363 (1992).
- [57] J. Gough and M. R. James, Automatic Control, IEEE Transactions on **54**, 2530 (2009).
- [58] O. Astafiev, A. M. Zagoskin, A. Abdumalikov, Y. A. Pashkin, T. Yamamoto, K. Inomata, Y. Nakamura, and J. Tsai, Science **327**, 840 (2010).
- [59] A. A. Abdumalikov Jr, O. Astafiev, Y. Nakamura, Y. A. Pashkin, and J. Tsai, Phys. Rev. B **78**, 180502 (2008).
- [60] J. Koch, T. M. Yu, J. Gambetta, A. A. Houck, D. I. Schuster, J. Majer, A. Blais, M. H. Devoret, S. M. Girvin, and R. J. Schoelkopf, Phys. Rev. A **76**, 042319 (2007).
- [61] A. A. Houck, J. A. Schreier, B. R. Johnson, J. M. Chow, J. Koch, J. M. Gambetta, D. I. Schuster, L. Frunzio, M. H. Devoret, S. M. Girvin, and R. J. Schoelkopf, Phys. Rev. Lett. **101**, 080502 (2008).